# Direct Digital Manufacturing Initiative

# Final Report

**Prepared under:**

**NCMS Project No. 140934 and**
**Cooperative Agreement HQ0034-15-2-0007**
**for the**
**Commercial Technologies for Maintenance Activities (CTMA) Program**

**March 2022**

**National Center for Manufacturing Sciences**
**3025 Boardwalk**
**Ann Arbor, Michigan 48108-3230**

.

# Table of Contents

**Section** **Page**

# List of Figures

**Figure** **Page**

# List of Tables

**Table** **Page**

# Acronyms and Abbreviations

| Term | Definition |
|---|---|
| 3D | Three-Dimensional |
| AM | Additive Manufacturing |
| CAD | Computer-Aided Design |
| CCDC | Combat Capabilities Development Command |
| CTC | Critical to the Customer |
| CTQ | Critical to Quality |
| CTMA | Commercial Technologies for Maintenance Activities |
| DDM | Direct Digital Manufacturing |
| DFM | Design for Manufacturing |
| DMLM | Direct Metal Laser Melting |
| DMWR | Depot Maintenance Work Requirements |
| DOD | Department of Defense |
| DOE | Design of Experiments |
| dX | Delta X |
| dY | Delta Y |
| FAA | Federal Aviation Administration |
| FARA | Future Attack Reconnaissance Aircraft |
| FLRAA | Future Long-Range Assault Aircraft |
| FPI | Fluorescent Penetrant Inspection |
| FVL | Future Vertical Lift |
| HIP | Hot Isostatic Pressing |
| IBIF | Industrial Base Innovation Fund |
| IR | Infrared |
| ITE | Improved Turbine Engine |
| MRL | Manufacturing Technology Level |
| NAVAIR | Naval Air Systems Command |
| NCMS | National Center for Manufacturing Sciences |
| O&S | Operations & Support |
| ODASD-MR | Office of the Deputy Assistant Secretary of Defense, Materiel Readiness |
| PSEF | Propulsion Systems Evaluation Facility |
| QFD | Quality Function Deployment |
| ROI | Return on Investment |
| SPC | Statistical Process Control |
| SPS | Significant Process Substantiation |
| TRL | Technology Readiness Level |
| U.S. | United States |
| VSE | Vendor Substantiation Engineering |

# 1. Executive Summary

Helicopter weight, fuel consumption and Operations & Support (O&S) rising costs during service life are issues that face new as well as aging aircraft programs. However, traditional manufacturing process limitations inhibit part design changes and constrain meaningful improvements to legacy systems due to unacceptable risk and costs to qualify. Acquisition lead time is also an obstacle for maintenance activities. Having parts where and when they are needed is often a challenge, resulting in above acceptable levels of non-mission capable assets.

Direct Digital Manufacturing (DDM) is universally recognized as a disruptive and enabling technology with the potential to revolutionize manufacturing and production of costly and complex gas turbine aircraft propulsion systems. The aircraft and airline companies are taking a careful look at this technology. With the expense of purchasing new aircraft, it is critical that methods are investigated. The introduction of advanced manufacturing technologies is viewed as essential to improving the performance of turbine engines as well as to meeting the maintenance and sustainment requirements for current and future aircraft.

Funding for a collaborative effort between the U.S. Army and GE Aviation was secured through the National Center for Manufacturing Sciences (NCMS) Commercial Technologies for Maintenance Activities (CTMA) Program and the Office of the Deputy Assistant Secretary of Defense, Materiel Readiness (ODASD-MR).

This report covers the final phase of a four phase, $2.4M Army ManTech program to advance DDM and additive manufacturing (AM) processes for military turbine engines. Phases 1 and 2 were successfully completed for the Army Combat Capabilities Development Command (CCDC) Aviation & Missile Center while Phases 3 and 4 were successfully completed under this CTMA collaboration agreement.

The CTMA project enabled and optimized advanced AM processes for aerospace quality super-alloy engine components that will eventually contribute to reduced costs, reduced weight and improved performance for the Department of Defense (DOD) and the Department of Energy.

## 1.1 Results

The project laid the necessary groundwork for enabling a manufacturing capability that opens up a wide design space for improving performance, reducing weight, reducing costs and improving readiness. It also enables the flexible reconfigurable factory with the capability to respond to both standard production and surge production demands.

The capability to manufacture affordable aerospace quality DDM components was demonstrated and verified by the fabrication of sector and full-scale components for the T700 series of turboshaft engines used in the AH-64 and UH-60 helicopters. The use of DDM parts has a broad range of applications when used in place of conventionally manufactured components in gas turbines for propulsion, secondary power, aviation, marine, & ground vehicles, as well as industrial power generation applications.

While there were several important deliverables from this project, the main deliverable was the final single lot T700 DDM Swirl Frame manufactured on the ATLAS machine in IN718 that was delivered at the end of this program phase. During the manufacturing process development of the DDM Swirl Frame, important learnings were realized in the areas of complex part printing, support structure strategies and post-

processing activities (Section 3.2.3 of this report). In addition to the part manufacturing learnings, significant findings were also documented in the areas of surface finish impact on throughput, multi-laser stitch evaluation, and melt pool sensing (Section 3.2.2 of this report).

## 1.2 Benefits

Virtually every new turbine engine design and upgrade for the Army, Air Force and Navy will benefit from DDM in some form if an affordable source of components exists in time to support the weapons systems schedules. Each new generation of high-performance military systems demands improvements in thrust-to-weight ratio, fuel consumption, secondary power generation demands, and reliability to meet the increased mission requirements that warfighters set forth. Hundreds of millions of dollars are spent on product technology development for each new generation of engines to assure that these increases in performance are possible. In recent years investments for advancing manufacturing processes have not kept pace with the demands for the related technology improvements. Improvements in manufacturing process technology must be achieved with each new generation of engines for these challenging new designs to be manufactured with acceptable quality, cost, and delivery rate to meet the warfighter needs.

The Army ManTech program in collaboration through CTMA provided funding to facilitate taking the DDM technology from the lab (TRL4) to production ready (TRL6+) for the T700 Swirl Frame while also initiating the efforts to bring multi-laser and melt pool monitoring capabilities. A separate, follow-on Army ManTech program will further this work bringing multi-laser capability, at least for Concept Laser machines, to TRL6. This capability will allow for the Improved Turbine Engine (ITE) program as well as other DOD programs to see the full potential of this advanced manufacturing technology.

## 1.3 Technology Transition

While there is no transition plan for the component developed under this effort, many of the manufacturing developments made during this program, most specifically regarding multi-laser stitching and melt pool monitoring, are applicable to and will bring value to future DOD engine programs. In fact, multi-laser stitching and monitoring technologies are part of a follow-on ManTech program intended to benefit the ITE program.

## 1.4 Recommendations

It is recommended that the DOD and companies invest in DDM technologies to hasten its introduction to the aviation sector on a large scale.

## 1.5 Invention Disclosure

Invention Disclosure Report(s):

DD882 Sent to NCMS ☐
No Inventions (Negative Report) ☒

## 1.6 Project Partners

- U.S. Army – Redstone Arsenal
- GE Aviation
- National Center for Manufacturing Sciences (NCMS)

# 2. Introduction

## 2.1 Background

The CTMA project leveraged the results of the Army Advanced Industrial Base Innovation Fund (IBIF), contract W15QKN-12-2-0001, where GE demonstrated AM fabrication of components centered around a bearing housing, brackets, and a rear frame strut tube. In this project, GE examined more critical engine components and developed production capable hardware and processes. A key piece of the advancement of AM technology for turbine engine components is the "design for additive," where redesign of parts with the intent to take advantage of AM will allow for a less restricted design space, reduced weight, and enhanced performance. It lays the manufacturing process groundwork required for that next step.

## 2.2 Purpose

The objective was to advance DDM and AM processes for military turbine engines. Specifically, the goals were to provide advanced manufacturing processes and technologies supporting fabrication of aerospace quality components for turbine engines. The project addressed process barriers to enable affordable DDM/AM parts fabrication for Army and DOD aviation. For this project the process will be referred to as DDM.

## 2.3 Scope/Approach

The T700 engine was utilized as a platform for advancement of the DDM technology in turbine engines from a manufacturing readiness level (MRL) of 4 to an MRL of 6. While the T700 helicopter engine was the focus, the resulting benefits will be transferrable to various other military platforms such as the Future Vertical Lift (FVL), Future Attack Reconnaissance Aircraft (FARA), Future Long-Range Assault Aircraft (FLRAA) and all H-60 variants. The project involved a study on the effects of surface finish on throughput, multi-laser stitch evaluation, melt pool sensor stitching assessment, identification of a candidate part, DDM process development, validation, development of manufacturing plans, and the form & fit check-out of a single engineering class part via assembly on a single T700 engine. Additionally, Army ManTech, Naval Air Systems Command (NAVAIR), and GE Aviation have had discussions regarding the ground testing of the final deliverable Swirl Frame on a USN T700-401C engine at the Patuxent River Propulsion Systems Evaluation Facility (PSEF), a test facility.

# 3. Project Narrative

## 3.1 Technical Background

### 3.1.1 Candidate Part Selection

#### 3.1.1.1 Identify Candidate T700 Parts

When designing a part, design engineers must incorporate and optimize the design for the method of manufacturing. The design of today's helicopter engine has been optimized for conventional manufacturing methods such as casting and forging plus machining, but not for DDM. Still, it is possible to realize benefits by applying DDM to conventional geometry. First, a cost savings for certain conventionally designed parts can be realized with DDM through reduced tooling costs, reduced part count, reduced touch labor, higher yield, and reduced capital costs. Secondly, by optimizing for DDM, performance enhancements through improved design enabled by DDM can be realized along with design simplification. These performance enhancements are achieved through part consolidation and geometric design optimization. Under this ManTech and CTMA effort front-to-back evaluation of the T700-701D engine by GE Aviation design and manufacturing engineering teams was undertaken to identify the final T700 engine component for DDM development. The part selection involved component size, material type, complexity, criticality and business economics. They were also judged based on the ability to advance and leverage advanced engine design capabilities that could potentially increase performance for future warfighter engine programs.

A thorough engineering Quality Function Deployment (QFD) evaluation of the T700 engine platform to identify potential direct metal laser melting (DMLM) candidate components for development was completed during Phase 1 of the program. Outcomes from the 2013 IBIF program along with the results of other QFD evaluations were used as a starting point for the QFD. The QFD evaluation criteria included:

- Part complexity and DDM
- Current cost and potential for manufacturing cost and/or part count reduction
- Current reliability and design deficiencies which may potentially be resolved using additive
- Current and potential material(s) of construction
- Other engineering requirements

### 3.1.2 Task 1 – DDM Process Development

#### 3.1.2.1 Effects of Surface Finish and Throughput on Mechanical Properties

*Technical Background – Surface Finish*
Surface finish is critical to the performance of any parts in two main areas: 1) fatigue life of mechanically and thermo-mechanically loaded parts and 2) fluid flow where surface finish is either critical to fluid flow, such as airfoils, or is critical to deposit buildup, such as fuel and oil lines. The as-built surface finish of a DDM part can be relatively rough, anywhere from an $R_a$ of 250 micro inches (6.4 µm) for a vertical surface to 1500 micro inches (38.1 µm) for a downward facing surface. The surface finish of a downward facing surface can also be degraded through the use of support structure that are attached to the surface and which must be removed by mechanical and/or chemical means. The effect on fatigue life of the as-built surface finish can be on the order of 30-50% depending on the alloy (Figure 1). Surface finish can also affect fluid flow in piping systems where the friction factor, and hence the pressure drop across a piping system, increases with increasing Reynolds number for turbulent flow conditions (read heat exchanger applications).

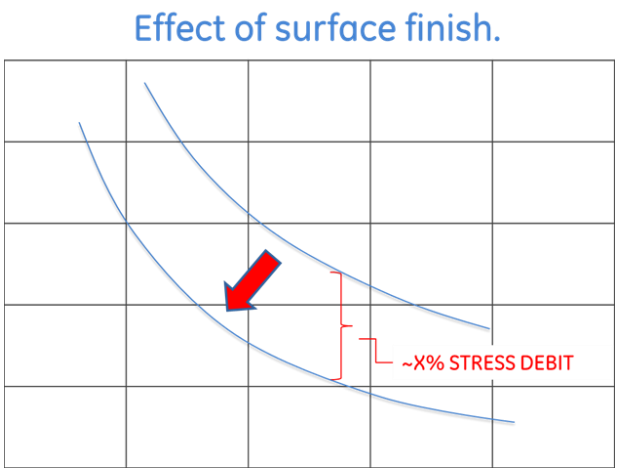


***Figure 1. Low Cycle Fatigue Material Curve***

The as-built surface finish of a powder-bed DDM processed part is a function of several process factors including layer thickness, build orientation, powder particle size and distribution, process parameters and scanning strategy. AM by definition is a layering process with typical layer thicknesses on the scale of 20-60 microns for the laser-based DMLM process to 200 microns for the electron-beam powder-bed process. The layering effect manifests itself as a directional roughness parallel to the build direction. It has been demonstrated that decreasing the layer thickness can improve surface finish but the effect on mechanical properties is yet to be characterized. The orientation of the build surface in relation to the build direction can also dramatically affect surface roughness. The upward and vertical surfaces tend to be the smoothest with surface roughness increasing with increasing degree of incline from vertical for downward facing surfaces. Unsupported downward facing surfaces can have the roughest surfaces due to the lack of solid material beneath the layer being exposed to the laser beam. Laser parameters and scanning strategies also affect surface finish by controlling the heat input and the resolution of the process with higher heat input and lower resolution conditions tending to increase surface roughness.

Because the as-built surface finish may be insufficient for some applications, post processing methods are needed to attain the desired finish. Surface improvement processes cover a broad spectrum but can be categorized into two major categories: additive and sub-tractive. The subtractive methods include abrasive machining, mass finishing, and electrical/electrochemical, while the additive includes electroplating, thermal spray, and slurry coating processes. The subtractive processes potentially improve the properties of the base material at the surface while the additive processes tend to maintain the physical characteristics of the base material surface while improving fluid flow properties through reduced drag.

*Surface Finish Survey and Critical Surface Identification*

In order to optimize surface finish for AM part application and engine integration, a surface finish effort was conducted that included evaluating in-process and post-process improvements. First, a surface finish technology was conducted, building on the survey con-ducted as part of the Army IBIF program mentioned earlier, for the post-process methods. In addition, new under this project, the survey was updated to include the latest on in-process surface improvement technology developments. The information was used to target the appro-priate surface finish requirements and surface improvement techniques.

*Surface Finish Parameter Development*

For in-process surface finish parameter development, a Design of Experiments (DOE) methodology was implemented to efficiently identify key process parameters.

*Technical Background – Throughput Enhancement*

Process throughput is a metric for this program and for the technology in general. The true benefit of AM is the design freedom enabled by the technology (i.e., the capability of producing geometry that cannot be produced any other way). However, this enabling capability must be both affordable and revenue positive. The

purpose of this ManTech program was not to unleash the enabling design freedom of additive but to advance the MRL of DDM from MRL3 to MRL6+ for components of the T700-701D engine family designed and optimized using the constraints of conventional manufacturing technologies. The constraints were that the implementation of DDM cannot change any mating interfaces nor have any detrimental effects on the performance of ancillary hardware or the engine itself. The intent was to justify the implementation of DDM based solely on cost and performance compared to conventional design and manufacturing technology.

Under the IBIF program, a path was identified to implement DDM on conventionally designed hardware that provided a cost savings on a time basis compared to conventional manufacturing processes with additional savings through improved yield, reduced manufacturing steps and reduced logistics. Savings could also be realized through reduced investment such as in capital equipment, manufacturing space and special work skills. One approach is to increase the amount of laser power available at the work piece in two ways: by increasing laser power and by increasing the number of laser scan heads on the DDM system. Increasing laser power is the simplest approach from a DDM system design standpoint but requires requalification of the material since this is considered a significant change to one or more key process parameters including laser power, scan speed, spot size, layer thickness and scan spacing. Increasing the number of scan heads on a DDM system is a much greater undertaking in terms of overall system design and complexity. Under the IBIF program, the proposed scenario of doubling the laser power and increasing the number of scan heads from one to four would effectively result in an 8X improvement in throughput over the baseline 200W, single scan head system. This is technically feasible since the lasers themselves are commercially available up to 50 kilowatts of laser power and because DDM powder-bed systems are available with up to one kilowatt of laser power. The use of multiple scan heads is not new. Dual scan heads have been available on plastic DDM systems for over a decade, with up to four scan heads per system being offered for the metal powder-bed DDM systems within the past several years.

### 3.1.3 Task 2 – DDM Plan Development

#### 3.1.3.1 Vendor Substantiation Engineering/Significant Process Substantiation (VSE/SPS) Plan Development

*Technical Background*
Along with the required drawings and computer-aided design (CAD) models required to produce a part, additional manufacturing documents are required. These documents, known VSE/SPS documents must be created for each specific part.

*VSE/SPS Plan Development*
Determination of the final part post-printing requirements for the additive T700 Swirl Frame were performed under this task. These requirements include fluorescent penetrant inspection (FPI), pressure check, cleanliness, as well as other activities. Additional requirements specific to AM were also identified and included as required. These are detailed in Section 3.2.3.1.

### 3.1.4 Industrialization Studies – Component Build Process Development

*Technical Background*
Design for DDM not only includes part specific design but also design for manufacturing (DFM). Although DDM releases the designer from the constraints of conventional manufacturing technology, there still are limitations, nuances, and unique constraints to each DDM process that must be accounted for in either the initial design of the part or in the build process itself. On the design side, for example, resulting mechanical properties and surface finish may affect wall thickness

considerations and flow channel cross sectional area. On the manufacturing side, if surface finish is a critical criteria, then build orientation and post-process selection may be affected. Even when many of these issues have been resolved pre-process, the dimensional accuracy of the DDM processes tend to be geometry dependent and require a series of test builds to "dial in" the process. This dialing in process is an iterative process and can take as few as a single build or multiple builds depending on the complexity and size of the part. After each build, the parts are evaluated for dimensional accuracy and overall part quality. The non-conformances are documented, adjustments are made, and the process is repeated until the part meets the requirements. It is also possible that the part design might be altered to accommodate the process limitations.

*Build Optimization Trials*
Under this program, the part selected, T700 Swirl Frame, was subjected to the build optimization process: build, inspect, modify, and repeat.

## 3.2 Technical Progress Completion

### 3.2.1 Candidate Part Evaluation and Selection

The core team met during the early part of Phase 1 to determine how to set up the QFD and what the Critical to the Customer (CTC)/ Critical to Quality (CTQ) should be and how they should be weighted. There was significant discussion at the team meetings on whether the weightings should favor a big stretch in improving the manufacturing process for additive, or whether the focus was to clearly advance/learn how to move from MRL4 to MRL6 for an additive part on the T700 engine. A meeting with the Army helped clarify that the GE team should make sure there was high confidence that the first part picked for the program would reach MRL6. Following the Army guidance about the focus being less about stretch and more about learning the process to move the MRL from 4 to 6, the CTQs were determined for the QFD, which had a strong focus on the Return on Investment (ROI).

Following this, the QFD and weighting was reviewed with the Army. After receiving Army approval of the CTQs the core team selected parts that would be scored in the QFD. The following process was used to downselect parts to be scored.

- Eliminate Chapter 5 (or commercial) safety critical parts
- Eliminate parts less than $1,000
  - Very difficult to show a reasonable ROI
  - Parts can be included as part of an assembly
- Eliminate hot flowpath parts
- Part size
  - Must meet current additive machine size capability
- Look at assemblies and subassemblies
  - Eliminate parts that cannot be combined due to material property restrictions
  - Expand subassembly and assemblies by looking at cross section and see if adjoining parts can be combined into the assembly with additive

Next the GE core team finalized the part selection for the QFD using the process detailed above. Table 1 shows the selected parts.

**Table 1. Parts Selected for QFD Scoring**

| |
|---|
| Bsump |
| Bsump + Heat shield |
| Combined c-sump/exh. Frame |
| Combustion Liner |
| Csump Assy |
| Diffuser |
| Diffuser/deswirler case |
| Exh Frame |
| Front Frame |
| HPC Case |
| Inlet Swirl Frame assy |
| Main Frame |
| Mid-frame assy |
| ODA Housing |
| VG Torque Shaft |

After completing the part selection, all the parts were scored in the QFD. The top scoring parts were all three sumps, and the Inlet Swirl Frame assembly. An in-depth review of all these parts was performed to determine a more accurate ROI with one or two parts downselected for final review. The downselect completed for each part included a summary sheet for each part that included:

- Material
- # Parts consolidated
- # In-house manufacturing steps completed
- Conventional cost
- DDM should-cost (250$^{th}$ engine)
- Projected savings/engine
- Project savings/year
- ROI (includes P&E estimate)
- Breakeven quantity

After reviewing it was determined that the ROI was best for the Inlet Swirl Frame as it had the greatest opportunity to reduce the number of parts and the number of operations. For the Swirl Frame the number of parts was reduced from 147 to 25. There are 122 parts consolidated with the unconsolidated parts consisting of nuts and threaded inserts only. In addition, there were 926 manufacturing steps eliminated by producing the part using the DDM process. Based on the above, GE and the Army teams agreed that Inlet Swirl Frame (6053T29G01) was the part chosen for this project.

## 3.2.2 Task 1 – DDM Process Development

### 3.2.2.1 Effects of Surface Finish and Throughput on Mechanical Properties

Goal of this work was to develop a parameter set to maximize throughput without degrading surface finish which was known to be a major contributor to fatigue life reduction. In Phase 1, an initial brainstorming exercise was conducted to define a strategy for achieving this goal. Approaches for improving throughput were evaluated as to the potential build time savings, technical and schedule challenges, and potential impact on surface finish and fatigue life. In general, most changes that would enhance process throughput would lead to a degradation of surface finish and fatigue life. The studies performed under this task would try to maximize throughput while minimizing the effect on surface finish. The study parameters are summarized in Table 2.

The general approach taken in this work was as follows:

1. Benchmark current parameters for surface finish, density, and build throughput.
2. From a series of screening builds, identify an increased laser spot size that shows promise for increasing throughput without an unacceptable loss of resolution or surface finish/fatigue life.
3. Optimization of process parameters for throughput with minimum surface finish impact with a 400 W laser and spot size identified in Step 2 through a series of statistically designed experiments.

**Table 2. Summary of Potential Approaches to Improving DMLM Throughput**

| Description | Time Savings | Risk | | |
|---|---|---|---|---|
| | | Technical | Schedule | Surface Finish/ Fatigue Life |
| Stripe Width Changes | Low | Low | Low | Equivalent |
| Multiple lasers | Very High | High | High | Equivalent* |
| Increase Hatch Spacing with Defocus | Medium to High | Medium to High | Medium | ↓ |
| Increasing Hatch Speed | Low to Medium | Medium | Medium | Equivalent* |
| Concentric Scanning | Medium | High | High | Equivalent |
| Reducing support scan time | Medium | Low to Medium | Low | ↓ |
| Increasing laser spot size | Medium | Medium | High | ↓ |
| Increasing Layer thickness | Medium to High | High | High | ↓ |
| Reducing contours | Low | High | High | ↓ |

A series of standard test parts was used for these studies. A detailed experimental design framework for parameter optimization was developed based on fractional factorial designs and a method of steepest ascent/descent. Factors evaluated included:

1. Hatch laser scan speed
2. Hatch scan spacing
3. Contour laser power
4. Contour laser scan speed
5. Downskin hatch laser power
6. Downskin hatch laser scan speed
7. Downskin hatch laser scan spacing
8. Downskin contour laser power
9. Downskin contour laser scan speed

The fractional factorial design allows the response surface relative to a large number of machine settings to be evaluated with a minimal number of test specimens. In this case, a single replicate required 32 specimens to be built. Three replicates were built with four center points for a total of 100 specimens.

A desirability score or similar measure was used to evaluate the results relative to multiple CTQs, which included:

1. Throughput
2. Surface finish/fatigue (90-degree surface)
3. Downskin surface finish/fatigue (45-degree surface)
4. Downskin surface/finish/fatigue (60-degree surface)
5. Downskin surface finish/fatigue (large radius through-hole)
6. Downskin surface finish/fatigue (small radius through-hole) and porosity

Because the process parameters have different impacts on each of these CTQs, a simultaneous optimization process was necessary. For example, it was expected that the parameter set that provides the lowest value of porosity may make it impossible to achieve desired downskin surface finish. Different test parts were required to measure each of these quantities.

The general approach to simultaneously optimizing the *y's* or outputs of the process relative to the process parameter inputs (*x's*) was as follows:

1. Measure each *y* for samples in single DOE. This will be a large fractional factorial.
2. Evaluate responses for curvature. If significant curvature is observed, axial points will be added to the DOE and corresponding samples build before continuing.
3. Convert y's to individual desirability score, $0 \leq d_i \leq 1$.
   - Specific formulas for calculating desirability scores are as follows:
     - If objective or target T is a maximum value

$$d = \begin{cases} 0 & y < L \\ \left(\frac{y-L}{T-L}\right)^r & L \leq y \leq T \\ 1 & y > T \end{cases}$$

       L is lower limit value

     - If objective or target T is a minimum value

$$d = \begin{cases} 1 & y < T \\ \left(\frac{U-y}{U-T}\right)^r & T \leq y \leq U \\ 0 & y > U \end{cases}$$

       U is upper limit value

     - Two-sided desirability function with target T between upper (U) & lower (L) limit

$$d = \begin{cases} 1 & y < L \\ \left(\frac{y-L}{T-L}\right)^{r_1} & L \leq y \leq T \\ \left(\frac{U-y}{U-T}\right)^{r_2} & T \leq y \leq U \\ 0 & y > U \end{cases}$$

   - If response $y_i$ is at goal or target, $d_i$ is 1
   - If response $y_i$ is outside acceptability limit, $d_i$=0
   - Weighting score, r, determines how quickly $d_i$ approaches 1
     - Use $r_i > 1$ for most important $y_i$'s (must get closer to target for $d_i$ to approach 1
     - Use $0 < r_i < 1$ for to de-emphasize importance of $y_i$
4. Calculate composite desirability score, D

   $D = (d_1 d_2 \cdots d_m)^{1/m}$ for m responses (y's)
5. Select *x's* to maximize D

Decision – Finally, an evaluation was made as to whether an optimum/acceptable parameter set had been found. If not, a new center point for a subsequent DOE was selected at the edge of the response surface corresponding to the best D value found and the process repeated.

Evaluation of the relevant CTQs measurement statistics from the parts, including porosity and surface finish was completed. Porosity data is illustrated in Figure 2 as a function of hatch speed and spacing. Porosity was not surprisingly statistically independent of contour and downskin parameters. An increase in porosity was observed as hatch scan speed and spacing (and consequently throughput) was increased. These values in conjunction with measures of surface finish and throughput were used to determine desirability scores which enable the process optimization process.

Throughput for each parameter set of the DOE was evaluated from the build time estimate for the part sector build. The parameter space that yields the best porosity in Figure 2 gives the longest build times in Figure 3. In both figures, the dashed line represents the process space where porosity is acceptable in the as-built state and can be safely removed in a hot isostatic pressing (HIP) process. As expected, hatch speed and spacing were found to be the primary drivers of build time.

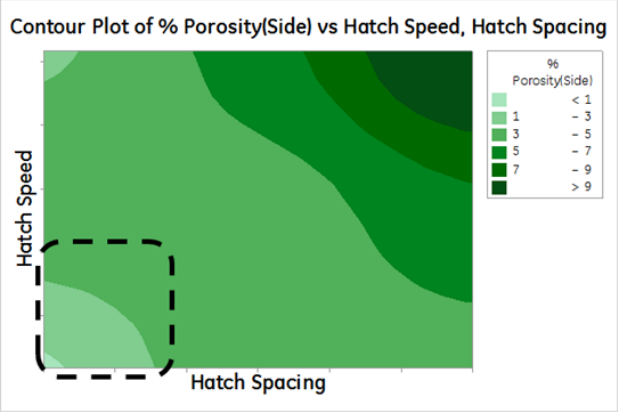


***Figure 2. Porosity Measurements as Function of Hatch Speed and Spacing from First Fractional Factorial DOE***
*The region in the dashed box represents the regime of acceptable porosity in the as-build state, i.e., porosity that can be safely removed in the HIP process*

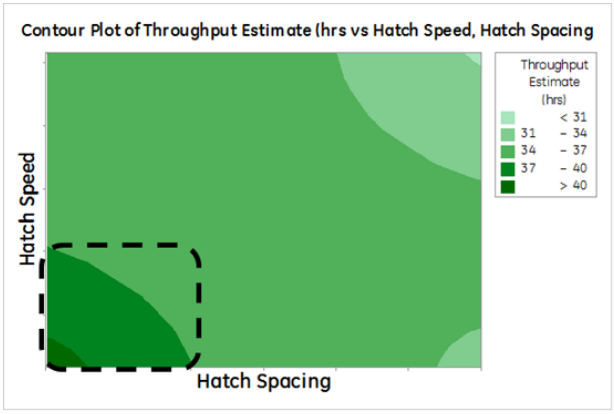


***Figure 3. Throughput Estimate for Swirl Frame Sector Builds as Function of Hatch Speed and Spacing***
*The region in the dashed box represents the regime of acceptable porosity in the as-build state, i.e., porosity that can be safely removed in the HIP process*

Several surface finish measures were also evaluated. Before proceeding with further optimization of the bulk hatch speed and spacing based on the results illustrated in Figure 2 and Figure 3, it was important to confirm that these parameters did not control surface finish, in particular on downskin features. This was indeed confirmed.

Key takeaways from the first fractional factorial DOE builds include:

- Identification of a process window where bulk parameters have minimal impact on surface properties
- Bulk hatch speed and spacing controlling factors for:
  - Porosity
  - Throughput
- Tradeoff between porosity and throughput
  - Parameters that give best throughput give unacceptable porosity
  - Parameters that give best porosity give lowest throughput

The second DOE was done in two parts: DOE2a to provide a closer examination of the process window for bulk parameters (illustrated by the dashed box in Figure 2 and Figure 3), and screening DOE2b to assess potential contour and downskin parameters. These two DOE were combined into a single build. DOE2a utilized a central composite design allowing curvature in the porosity response to be evaluated. Only bulk hatch speed and spacing were varied in the DOE which included three replicates of the design with three center points for a total of 27 porosity cylinder samples. Ultimately, the goal was to select a hatch speed and spacing setting as close to the upper right corner of the process window shown in Figure 3, representing the highest throughput. For each set of process conditions, the standard deviation of the porosity response was also calculated. Conditions where the mean porosity plus three standard deviations exceeded 5% were eliminated from consideration as this represents the HIP removal limit. The fastest two combinations of hatch speed and spacing that met this criterion were selected as parameter sets for the next build. The results of these builds showed a mean porosity of 0.9626% as seen in Figure 4. This resulting distribution shows that the porosity using these parameters is unlikely to approach or exceed 3% (5% being

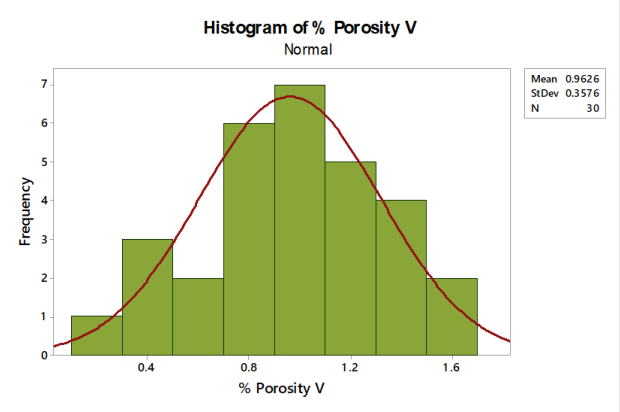


***Figure 4. Histogram of Percent Porosity for Gage Study Build***

the approximate HIP removal limit) which means that the porosity should be healed by HIP process. The next step was to ascertain if the new parameters caused significantly more distortion jeopardizing potential to meet geometric tolerances. Initial distortion modeling indicated that the degree of geometric distortion expected with the new parameters was not significantly different from that of the existing parameter set. Note that an assumption was made that the weld penetration depth was the same as that of the existing parameter set which may impact the accuracy of this conclusion. Nonetheless, the modeling results provide a degree of confidence moving forward with parameter development work. The next steps were DOE studies to optimize contour and downskin parameters as part of surface finish enhancement. The first of these was a full factorial focused on contour power and speed to minimize surface roughness on vertical and near vertical surfaces. An additional DOE study involved a fractional factorial focused on downskin hatch power, downskin hatch speed, downskin hatch spacing, downskin contour power, and downskin contour speed to minimize surface roughness on different downfacing surfaces.

As mentioned above, the next steps were DOE studies to optimize contour and downskin parameters as part of surface finish enhancement. One build was completed to establish a baseline on surface finish for an existing GE parameter set for this material (IN718). For 90-degree and 60-degree surfaces from the build surface, mean Sa values of 286 and 757 µin respectively were observed in this build. Two contour DOE were performed to optimize surface finish on vertical and near vertical surfaces, labeled DOE3a and DOE3b. These and included contour power, speed, and beam offset as factors. The best surface finish was observed at the lowest settings for beam offset, scan speed, and laser power used in the DOE. Because of the selected beam offset value where the best surface finish was observed, it was deemed that there was a risk of sub-contour porosity. Cutups of samples were examined, and sub-contour porosity was indeed observed, as illustrated in Figure 5.

As mentioned above, DOE4 utilized a central composite design extending from the low power speed, and beam offset parameter space identified to yield the best surface finish in DOE3a. Including center points in the design, a total of 51 samples were created in this build. Sa values for the near vertical surface (60-degree from the build plate) are illustrated in Figure 6.


***Figure 5. Illustration of Sub-Contour Porosity in Low Sa Sample from DOE3a***
*Sub-contour pores are circled in yellow*

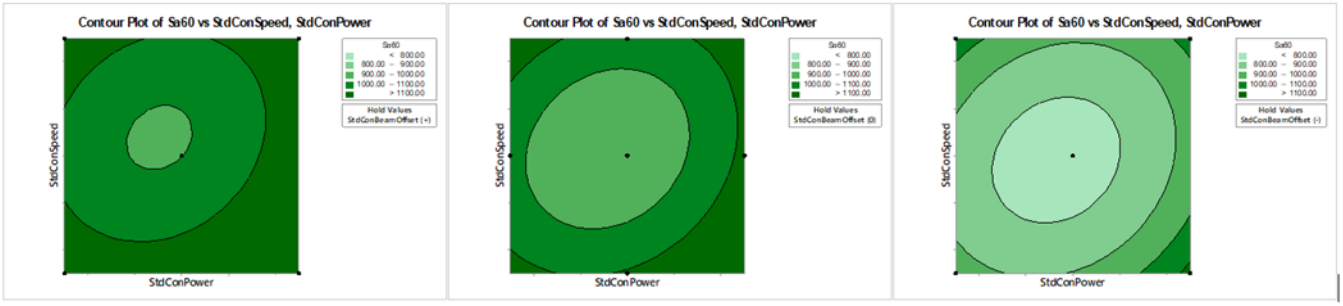


***Figure 6. Sa Values on Near Vertical (60-degree from build plate) Surfaces for DOE4 for High (left), Center Point (middle), and Low (right) Values of Beam Offset***

A clear optimum near the center of the power and speed parameter window examined was observed on the near vertical surface with best results at the lowest value of beam offset examined. Moving further into the negative beam offset space would likely introduce sub-contour porosity that could not be healed with a second post-contour and would not be attempted in this work. The mean Sa value for samples made with these "best" parameters was not statistically different from the current standard GE parameters with comparable variance.

Sa values for the vertical surface (90-degree from the build plate) are illustrated in Figure 7. Lowest values were observed in the high power/ low speed regime for the lowest beam offset setting. Sa values were significantly higher than those observed in the baseline, established GE parameter set. Further optimization could be achieved by moving into lower beam offset or lower speed/higher power settings, however, this would result in higher Sa values for the near vertical surface (60-degree from the build plate) as shown in Figure 6.

Overlaying the contour plots for the low beam offset values from Figure 6 and Figure 7 provides an illustration of the optimal contour parameter space and is shown in Figure 8. A parameter set in this regime was chosen and used for the next set of experimental builds.

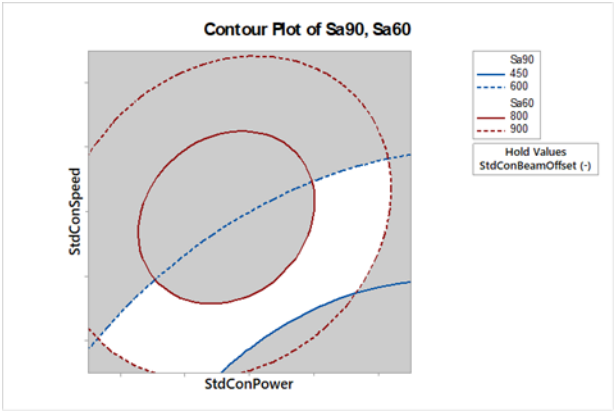


***Figure 8. Overlay Sa Values on Vertical (90-degree from build plate) and Near Vertical (60-degree from build plate) Surfaces for DOE4 for Low Values of Beam Offset***
*Area in white is optimal for both surface finish metrics*

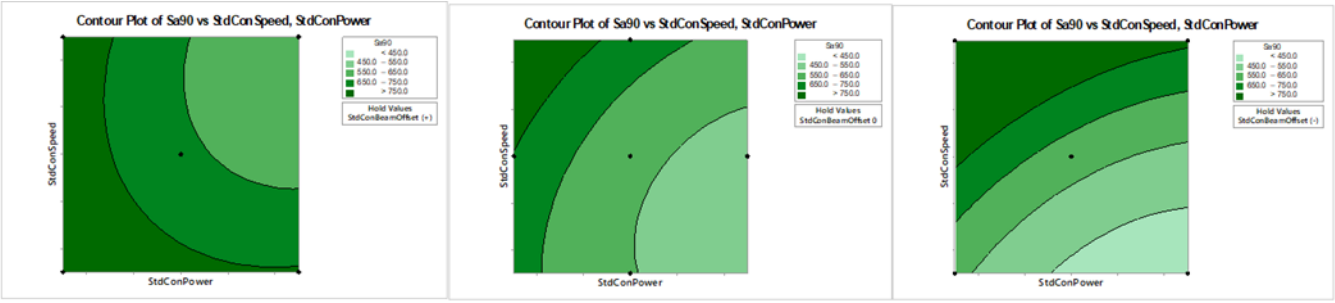


***Figure 7. Sa Values on Vertical Surfaces for DOE4 for High (left), Medium (middle), and Low (right) Values of Beam Offset***

Recall that a parameter set in the optimal contour parameter space (shown in Figure 8) was chosen and used for the next DOE (DOE5). DOE5 focused on a second post-contour's ability to heal sub-contour porosity without adversely impacting surface finish. In the regime examined in DOE5, a slight degradation of surface finish was seen. Additionally, this DOE was only partially successful in healing the sub-contour porosity. It was healed below the 60-degree surface but not below the 90-degree surface. This means that further study would be required to further optimize this second post-contour. A summary of all DOE is provided in Table 3.

**Table 3. DOE Summary**

| DOE# | Description |
|---|---|
| 1 | Bulk Screening |
| 2a | Bulk Dial-in |
| 2b | Contour/Downskin Screening |
| 3a | Single Contour Dial-in |
| 3b | Double Contour Dial-in |
| 4 | Sub-contour porosity healing screening |
| 5 | Sub-contour porosity healing dial-in |

*Conclusions*

For a given laser power, greater process variability was observed as the laser spot size was increased. Parameters that give lowest porosity typically result in poor surface finish. Bulk hatch parameters do not appear to be having a significant impact on downskin surface finish. Bulk hatch speed and spacing are the controlling factors for porosity and throughput. Throughput improvement is a tradeoff with porosity. The parameters that give best throughput give unacceptable porosity and conversely the parameters that give best porosity give lowest throughput. Increasing throughput must be balanced against quality needs.

### 3.2.2.2 Multi-Laser Stitch Evaluation

*Background – Multi-Laser Misalignment*

Large format multi-laser systems are a growing segment of the additive market and bring with them benefits of increased part size and build rate. With this capability comes a new type of error mode in the system, the misalignment of optical systems relative to one another. This misalignment could influence the quality of a printed part that bridges the optical system processing zones. Stitching is the interaction of optical systems at the scan path level to create a single cohesive part. Each layer will see two lasers operating along a single line, referenced as a stitch line, as shown in Figure 9. The stitch line will then shift slightly in a direction perpendicular to its length to avoid a repeated location of laser strike transient zones. These stitch lines can be introduced both parallel and perpendicular to the gas flow direction within the machine, following the *x* or *y* machine coordinate axes.

When introducing multi-laser stitching, the system adds a new type of process drift, the misalignment between each optical system relative to one another. Each individual optic train can be well aligned within its own coordinate frame, accurately lasing the process with the correct hatch spacings and offsets. The potential drift is the global migration of one laser relative to another, causing the scan strikes of differing optic trains to not match one another when processing a common local part build area. There are multiple scan strategies and parameters available in the build file generation process that can influence the stitching zone, through which the correct combination can add robustness against process drift. To build confidence in the machine architecture, it is important to identify what the machine process capability is, in this case the machine's laser-laser alignment, and the amount of allowable

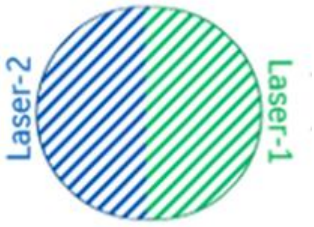


***Figure 9. Example Scan Path Stitch of Single Laser***

misalignment the machine can have without causing a detriment to material behavior.

The ManTech Multi-Laser Stitch Evaluation program has worked to identify the acceptable processing range to maintain material quality, as shown in the green region of Figure 10, and how the methodology of stitching can influence the process behavior. This is done through the creation of intentional misalignments in the system, simulating potential machine error modes between optical trains, and measuring the material response. An example is shown in Figure 11. Through the comparison of the material quality of these error modes with similar non-stitched parts, the team measured the shift found in material quality and at what misalignment level. Through exercising stitch variables, one can also identify potentially impactful settings that can add further resilience to the system against optic train misalignment.

*Procedure*

To build a process map relating optical train misalignments to a material response, multiple DOEs are required across several geometry features. If two optic trains are used to create the DOEs, with intentional misalignments added, the DOE variations will be confounded by the uncontrollable misalignments between the two systems. To produce consistent and exact misalignments, which is required for process map generation, any unintentional shifts must be minimized.

Leveraging a toolkit developed at GE Research, a designed build can be quickly assembled with varying stitch methods and misalignments added on a per-part basis. The Build File Generator Tool takes in the planned process parameters and scan paths, the stitch strategy with accompanying parameters, and the planned machine variation in the *x* and *y* directions listed in a text-based input table. The output of the program is a completed build file. Using the consolidated information of stitching variations added to the DOE Generator Tool in the form of the input table, resulting material characteristics can be combined for analysis once results are received from characterization.

*Experimental Work*

On an IN718 M2 Concept Laser system, two additive feature types were investigated, thin walls and downskins, with varying levels of sub-features. The identification and investigation of these features were critical to understand multi-laser stitching impact as they tend to derive larger shifts in melt pool and process behavior versus a bulk region, providing an opportunity for greater sensitivity to optic train misalignments. The material impact measured include internal void formation and external surface finish, in the as-built state.

*Thin Wall Stitching*

Thin walls in AM tend to operate in a processing regime more sensitive to melt pool variation than typical bulk feature, due to the constrained processing and thermal regions. With the introduction of stitching, which adds successive overlapping strikes and local areas of misalignment, this is a feature which may prove more sensitive to stitch error modes than bulk.

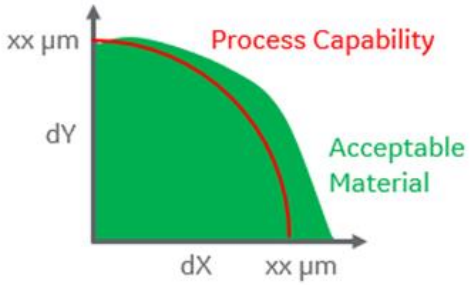


***Figure 10. Multi-Laser System Should Have Processing Capability Tolerances within Bounds of Allowable Material Quality***

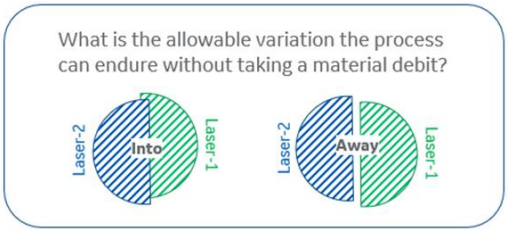


***Figure 11. Type of Misalignments that May Cause Different Material Shifts***

When conducting the thin wall stitching build trials, the feature space explored ranged from 0.5mm to 3mm wall thicknesses, both vertical and angled. A single part was designed to contain all wall thicknesses, with the vertical wall shown in Figure 12. The Vertical Thin Wall Sample contains wall thicknesses of 0.5, 0.75, 1.0, 1.5, 2.0 and 3.0mm, providing a single part to span thin wall types back to a bulk-like condition at the thickest feature. The vertical wall sample was stacked three tall with a solid section acting as a buffer between each segment. Using parts A, B and C to compile a single sample provided a stacked capability on the build plate, allowing more test conditions in a single print and reducing the total parts characterized. A second coupon type was generated using the same wall thicknesses, at a 40-degree angle, that was stacked two tall, generating a more extreme build condition while not triggering a transition to downskin parameters.

Each thin wall part (A, B and C) had a simulated laser stitch line incorporated along the width of the sample, with a layer-to-layer variance of the stitch being denoted by a Stitch Width. The orientation of the stitch line was consistent between all samples, but each stacked segment saw differing levels of simulated optical train misalignment.

Once printed, the sample was sectioned along the stitch plane and imaged as a mosaic. Each image was then sub-divided in two steps; first for each stacked part within the thin wall coupon, followed by individual files saved for each wall thickness. The individual wall thicknesses were then analyzed for void formations and surface finish.

*DOE Setup*

The thin wall DOE varied conditions concerning the application of stitch strategy across the part in addition to machine variation and errors that could have an influence on resulting stitch material quality. The following stitch parameters and machine error modes were leveraged in the investigation:

- Stitch Parameters:
  - Layer Increment Strategy
  - Stitch Overlap Zone Width
  - Stitch Strike Reprocessing
  - Part/Stitch Line Rotation
- Machine Variation:
  - Machine Error – dX, Shear
  - Machine Error – dY, Gap/Overlap

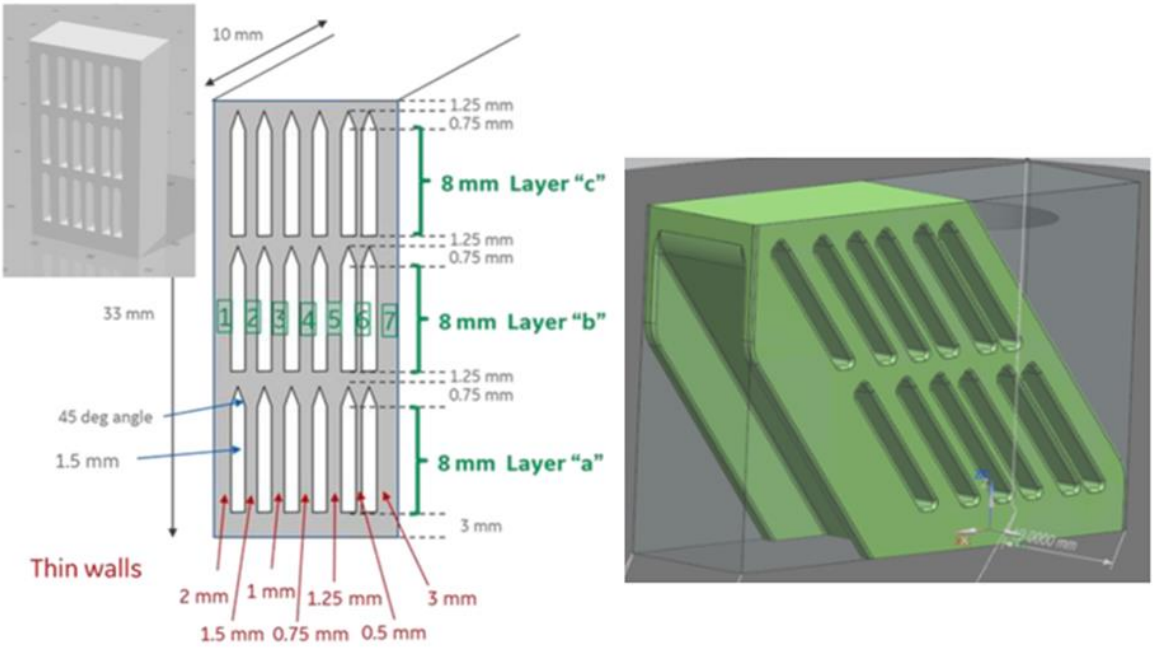


***Figure 12. Stacked Vertical (left) and Angled (right) Thin Wall Part for Consolidation of Print and Characterizations***

The stitch increment strategy dictated how the stitch would migrate layer-to-layer. To ensure any issue that can arise within the stitch region can be healed through the re-melt by the following layer, it is important to not have the stitch line at the same location over successive layers. The strategies investigated on this program are two methods to migrate the stitch region across layers. The stitch overlap zone width is the region of the part for which the stitch travels between layers, setting the boundary region that the Stitch Increment Strategy will traverse.

When applying a stitch to a part, each vector split between lasers had a set amount of overlap, or reprocessing, between the vectors to add robustness into the process. The total amount of reprocessing can vary, at the most extreme case being set to zero. The closer the setting is to zero the less both laser vectors will overlap with one another, allowing misalignments to begin leaving gaps in laser processing within the layer where powder can go un-melted. In build trials for this program, the reprocessing zone was held constant at a level near the parameter hatch spacing.

During setup a subset of parts were rotated, after scan path and stitch conditions had been applied, to identify if stitch directions parallel or perpendicular to the gas flow direction influence resulting material behavior. Machine error conditions, in both *x* and *y* orientation, were simulated optical train errors that introduced potential stitch misalignment conditions that may be found during regular machine operation. Delta X (dX) build conditions are translations between the optic trains along the x-coordinate direction relative to the machine coordinate frame, while Delta Y (dY) is the y-direction. For the selected part geometry, Delta Y shifts were applied in positive and negative directions as these caused two types of variation modes, gap and overlap stitch conditions. Delta X shifts were performed in one direction as the shear variation was mirrored across both sides. Due to part rotation being introduced within this program for impact assessment, misalignments were denoted by Shear or Gap/Overlap, introducing the error modes seen in Figure 13.

*Build Analysis*

The thin wall stitch study focused on two areas: as-built surface finish and porosity generation. For surface finish, tortuosity metrics were calculated using micrographs of each wall thickness. Tortuosity is the ratio of the length of the measured curve, in this instance the micrograph surface of the wall, divided by the distance between both ends. The rougher the surface, the higher the tortuosity value.

Stitch Orientation Influence on Surface Finish – The use of multi-laser systems can see the introduction of stitch lines along the *x* or *y* axis of the machine coordinate system, putting the stitch line parallel or perpendicular to the gas flow depicted in Figure 14. Using two sample

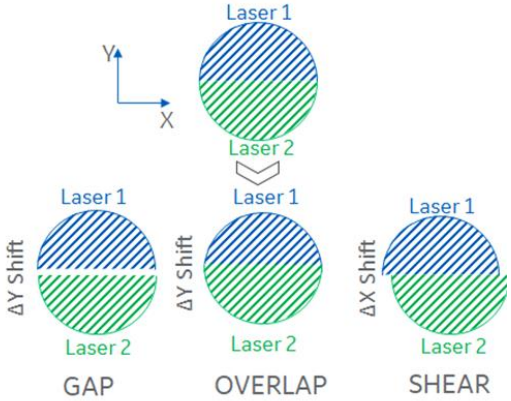


***Figure 13. Delta X and Delta Y Laser Misalignment Build Conditions***

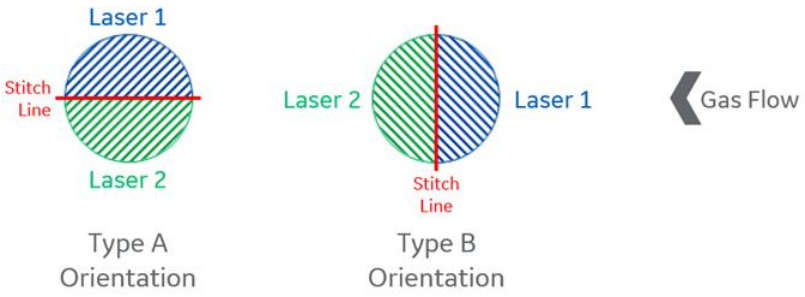


***Figure 14. Stitch Line Orientation Relative to Gas Flow Direction***

rotations on the build plate, offset by 90-degree, an impact on stitch orientation was considered.

Each side of the printed walls were assessed separately to reduce the influence of the surface direction relative to gas flow on stitched regions. Figure 15 compares the left side of thin wall segments to varying levels of shear stitch error, for both Type A and Type B orientations of the stitch relative to the gas flow direction. The Type B build style shows a higher indication of rough surface, marked by an increase in tortuosity, as the shear error increases in comparison to the Type A rotation. This result is further highlighted in Figure 16 when making the same comparison using the right side of the thin wall surface.

This provides an indication that stitch orientation relative to the build coordinate system can have an impact on resulting surface finish at higher levels of shear stitch misalignment. The shear error and part rotation in combination with the shear error show a statistically significant impact on the resulting tortuosity measurement. As reflected in Figure 15 and Figure 16, the Type B perpendicular orientation of the stitch line relative to gas flow and an increasing level of shear misalignment will increase the surface tortuosity.

The same comparison is then made of stitch direction, relative to gas flow, versus misalignment in the creation of gap or overlap conditions. Results shown in Figure 17 and Figure 18 of the gap/overlap stitch misalignment condition show a lower dependency of tortuosity to various levels of misalignment. While the variation is high across different stitch error conditions, there is no clear trend as either a gap or overlap conditions are generated.

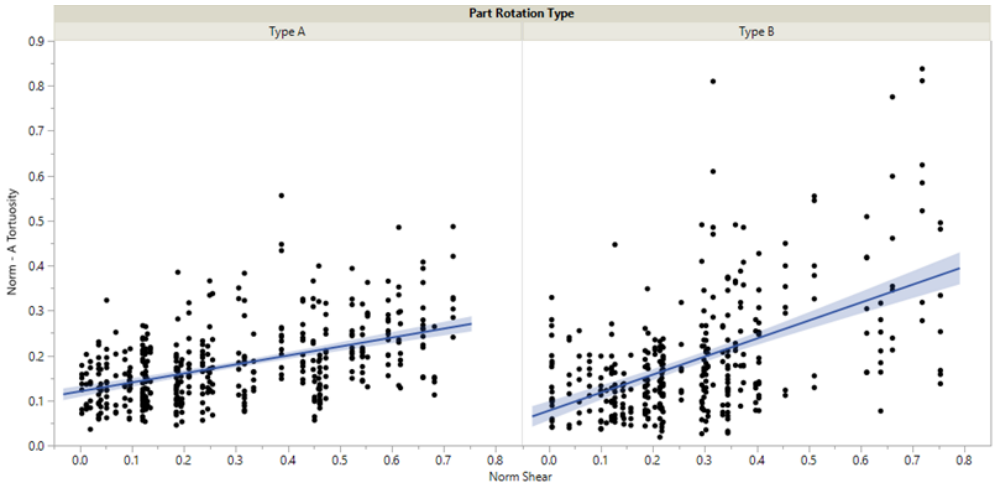


***Figure 15. Tortuosity versus Shear Displacement of Parallel, Type A (left) and Perpendicular, Type B (right) Stitch Alignment Relative to Gas Flow for Side A of Thin Wall***

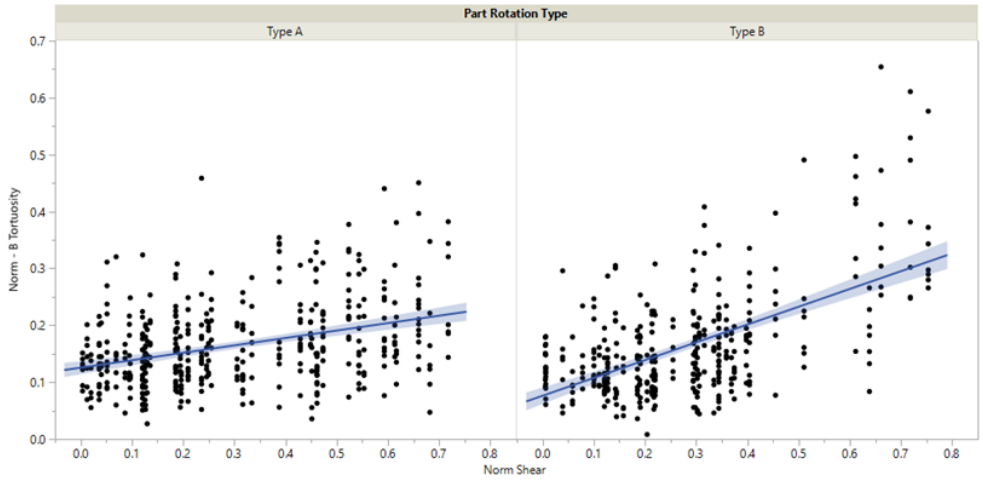


*Figure 16. Tortuosity versus Shear Displacement of Type A (left) and Type B (right) Stitch Alignment Relative to Gas Flow for Side B of Thin Wall*

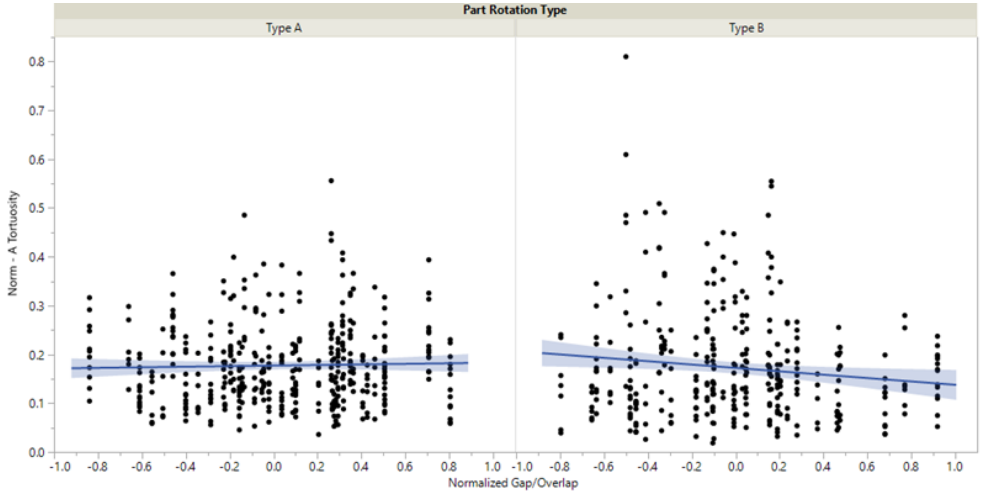


*Figure 17. Tortuosity versus Gap/Overlap Displacement of Type A (left) and Type B (right) Stitch Alignment Relative to Gas Flow for Left Side of Thin Wall*

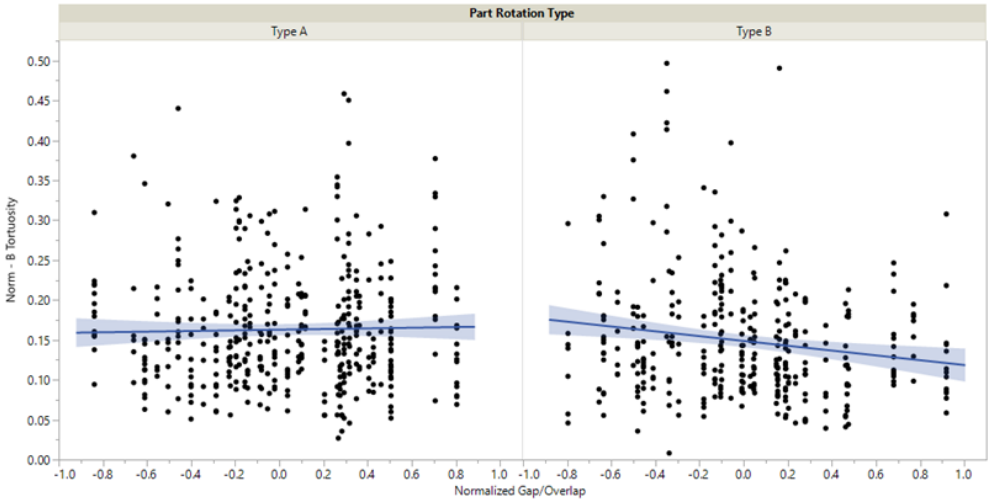


*Figure 18. Tortuosity versus Gap/Overlap Displacement of Type A (left) and Type B (right) Stitch Alignment Relative to Gas Flow for Right Side of Thin Wall*

Stitch Strategy Influence on Surface Finish – With an identification of varying stitch surface finish quality due to orientation relative to gas flow, an assessment was conducted using the worst-case Type B stitch orientation to ascertain if a unique stitch strategy provided more robustness to the process. Of all the stitch variables, the layer-based stitch strategy was found to influence process quality and provide a path to a more stable process.

Two types of stitch strategies were incorporated in the test matrix, changing how the stitch migrates between layers within the bounded stitch width, influencing the bulk and contour scans. The two stitch strategies explored the maximum distance the stitch line travels between layers; Type 1 allowing up to the stitch width while Type 2 minimized the travel distance. Figure 19 and Figure 20 assess the influence of stitch strategies relative to shear and gap/overlap stitch errors. Both sets of samples highlight a higher sensitivity to stitch errors with the Type 1 stitch strategy versus the Type 2 stitch strategy. The Type 2 stitch strategy shows higher robustness against large amounts of gap and overlap stitch error conditions, and a lessened impact against shear error versus the Type 1 condition.

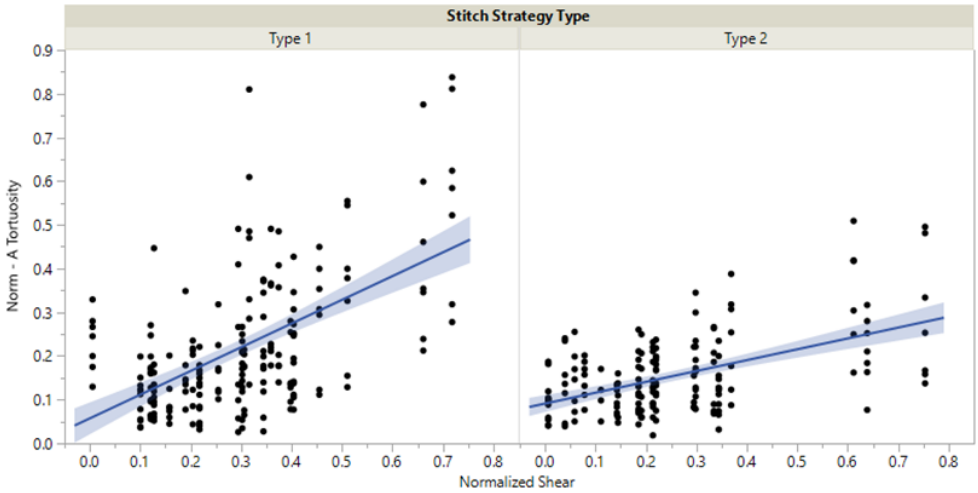


***Figure 19. Tortuosity of Left Side of Thin Wall versus Shear Displacement of Type B Oriented Part for Type 1 and Type 2 Stitch Build Styles***

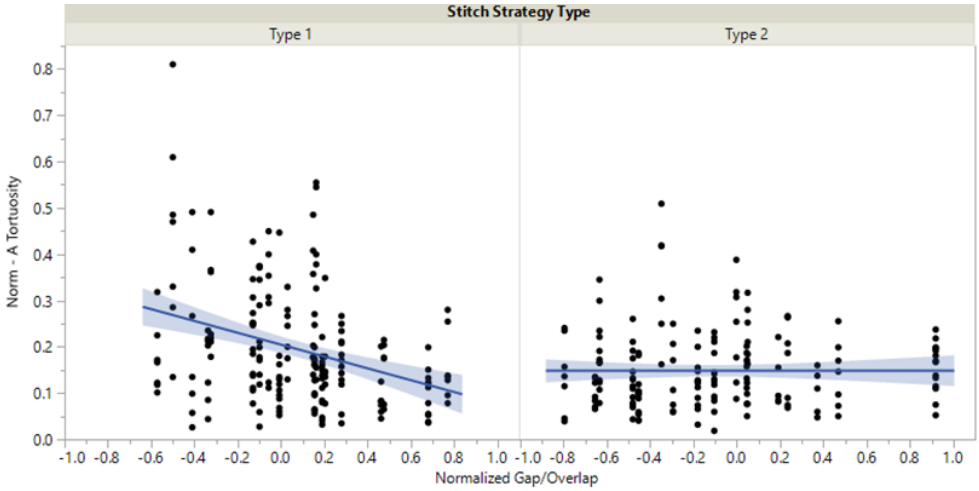


***Figure 20. Tortuosity of Left Side of Thin Wall versus Gap/Overlap Displacement of Type B Oriented Part for Type 1 and Type 2 Stitch Build Styles***

Material Response: Vertical Walls – During the assessment of varying wall thicknesses for interior material quality, it is important to differentiate each wall thickness from one another. When building on an additive system, the behavior of the standard parameter set can cause slight changes in resulting as-built voids within increasingly thin walls. A slight increase in material void formation can occur in a thinner wall versus a 3mm bulk-like feature. To properly assess the sensitivity of void formation relative to stitch conditions, it is important to normalize the material response versus a similar feature built without a stitch. For this assessment, each stitch misalignment for a wall thickness is compared against the mean-value material anomaly condition measured with the same wall thickness built without a stitch. Furthermore, all parts were printed on the same build to eliminate build-to-build variation.

The material response denoted on all material response plots are a comparison of the stitched part material condition relative to the no-stitch feature. A 1.0 ranking marks a nominal behavior that is not differentiated from a non-stitch condition, a >1 ranking marks an increase in the material response, while a <1 ranking would mark an improvement.

With the large influence of stitch orientation relative to gas flow direction being identified through the surface finish analysis, this was the initial area of investigation for void formation within the micrographs. Each wall was mapped against the two rotation types, offset by 90-degree, for a trend towards one having a higher material response. As shown in Figure 21, higher wall thicknesses found very little sensitivity to stitch orientation. Thinner walls highlight some variation in the material response between the Type A and Type B stitch orientation, but neither is found to be consistently trending across the wall thicknesses. Due to the higher variability found in the thinner walls of the analysis, this is potentially due to higher order effects and dependency on build plate location. Due to the limited data set, gas flow directions were combined for analysis and mapping, though this is a potential area to explore further in the future with increasingly thin walls.

The lack of a clear trend between stitch orientation relative to an internal material response is found to contrast with its impact on surface finish. This highlights that each stitch variable can impact material responses to varying degrees. To better visualize the impact of stitch misalignment conditions relative to the material behavior, response surface plots were generated for each wall thickness, mapping the shear and gap/overlap stitch misalignment error conditions on the *x* and *y*-axis respectively.

When assessing stitch features on the resulting material response the most prominent identified

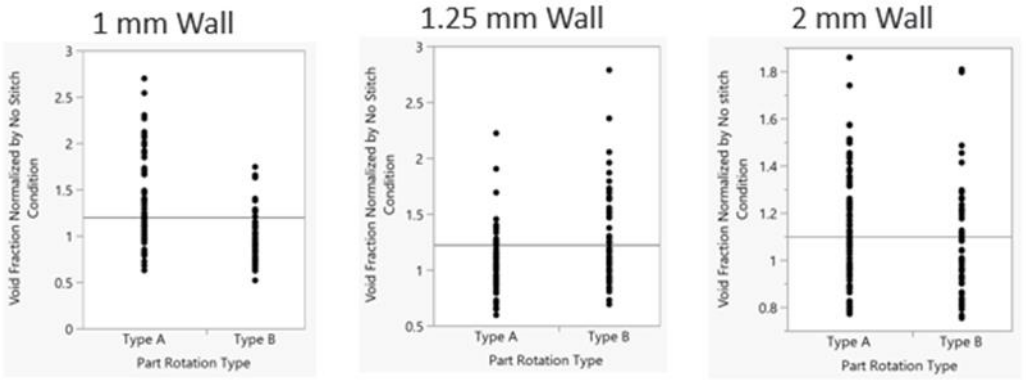


***Figure 21. Material Response of Three Wall Thicknesses Against Two Types of Stitch Orientation Relative to Gas Flows***

is the stitch width, controlling the region of a part that a stitch can traverse layer-to-layer. This is highlighted when assessing a stable processing condition of a 3mm wall thickness, as shown in Figure 22, with a large and small stitch width. A large stitch width provides a robust build regime, with the material response never straying far from the no-stitch material quality, even at the most extreme stitch misalignment build conditions. When similar misalignments are applied to a smaller stitch width 3mm feature, several higher void formation regions occur within the space.

When the same wall thickness is assessed for a screening analysis, both shear stitch error and stitch width reside as the largest contributors to the void fraction increase shown in the response surface curves a 3mm example shown in Figure 23. Similar results were found across all wall thicknesses, some providing a less distinct step between each quality metric than shown in the figure, with both misalignment conditions and the stitch width as the leading influencers to the variation in material quality. Through the identification of a larger stitch width, the team had an opportunity to reduce the overall material shift as the misalignment conditions were applied to a part feature.

Using the large stitch width, providing a more robust build at varying levels of misalignment, one can still see increasing sensitivity to the stitch error as wall thicknesses reduce in size. When approaching thinner wall conditions potential scan path errors introduced through the shift in dX and dY optical train misalignments in combination with potentially more sensitive build features led to an increase in the void fraction amount relative to the no-stitch condition. As shown in Figure 24, the 1mm wall thickness has higher variability across the optic train misalignment space than you find in a bulkier feature.

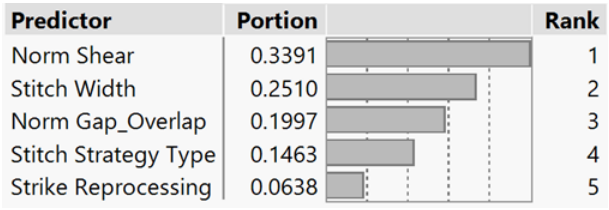


*Figure 23. Predictor Screening of 3mm Wall Thickness for Main Effects with Stitch Orientation Type B*

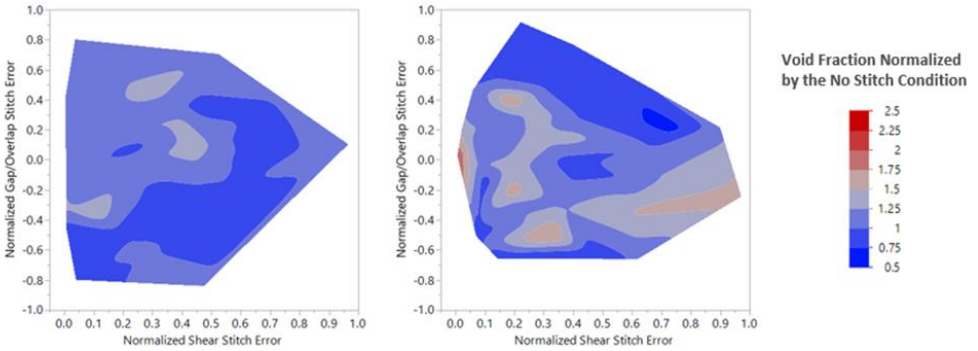


*Figure 22. Void Fraction within 3mm Thick Wall Using Large (left) and Small (right) Stitch Width*

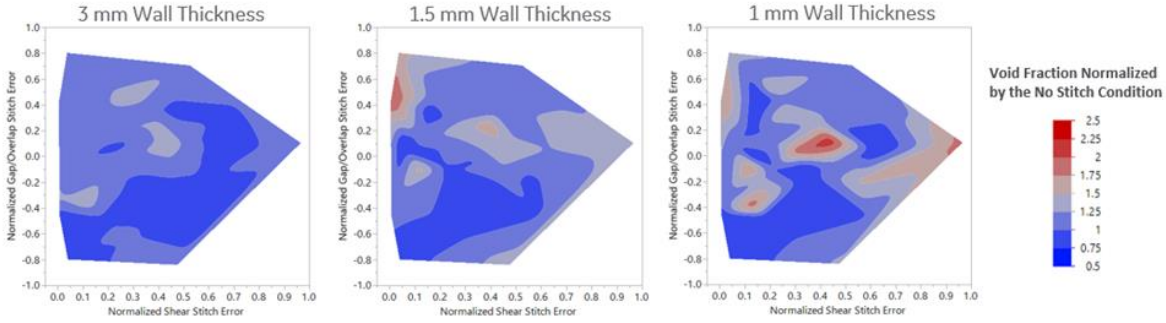


*Figure 24. Void Fraction Amounts Relative to No-Stitch Conditions of 3, 1.5 and 1mm Wall Thicknesses*

Several key learnings were generated during the thin wall assessment of the material response, relative to the corresponding no-stitch condition. Bulk regions, or wall thicknesses that approach a bulk-like condition, are robust to even large levels of optic train misalignment made even more so by basic optimization of the stitch feature. As thinner walls are built with similar optic train misalignments, the chance of variation in the material response increases.

Material Response: Angled Thin Walls – A subset of stitch misalignment conditions were applied to angled thin wall regions using the standard part parameter set already applied to the vertical thin wall regions for material void fraction analysis, primarily exploring their susceptibility to material behavior shift with the introduction of shear and gap/overlap optic train misalignment conditions. The resulting material behavior was found to be more resilient to stitch misalignment than the vertical wall sections. The parts tended towards high density and did not exhibit the same process behavior seen in the vertical wall segment.

Likely, the cause of increased process robustness was due to the migration of the thin wall edge throughout the *z*-direction of the build. The most problematic regions identified in the vertical walls were those around the contour and contour-bulk transition zones, which were consistently aligned every layer with the traditional geometry. By tilting the thin wall, the migration of the processing zone each layer allowed better remelting and correction of any stitch errors introduced in the process.

*Downskin Stitching*

Downskin, or overhanging, additive regions are a part feature that typically introduces large amount of surface finish variation relative to a vertical part segment, caused by greater instability in the melt region through laser processing applied away from underlying solid metal and through limited heat dissipation over time. Due to these variations in the downskin feature, unique build parameters are typically applied to minimize the material response. Reduction in the energy applied beyond angles of 45-degrees, with further mitigations implemented at even more extreme angles, the surface region of the parts are able to be built with greater consistency, though not reaching the surface quality of a vertical wall.

Due to the development of unique parameters that can process over exposed powder regions and reduce the total thermal load applied to the edge of the part, the same region can be more robust than the vertical section against further incurred surface finish debits when optic train misalignments are applied. As shown in Figure 25 the introduction of a stitch error was, at worst, furthering the overhang condition for which the downskin region was already compensating. If the error was in the opposing direction, reducing the amount of overhang, the process would instead tend towards a bulk processing condition. Given the stitch transition created this condition for a single layer before resuming normal overhang processing, the risk of under processing is minimal and no impact was seen in the material response.

*DOE Setup*

To test the downskin region with stitch misalignment conditions, a 16.5mm geometry was designed with three discreet angles at 45, 35 and 25-degrees from horizontal. A stitch was

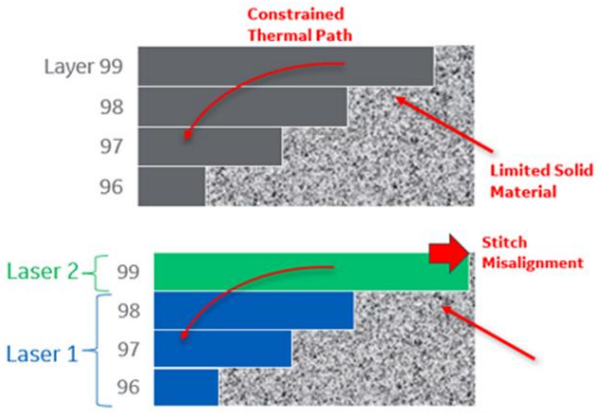


***Figure 25. Processing Conditions of Typical Downskin Region (top) and Downskin with Stitch Error (bottom)***

introduced to each part along the centerline, denoted by the red plane in Figure 26, with a stitch width highlighted in blue. The part was designed to stack multiple angles with increasingly extreme downskin conditions in the *z*-direction, limiting the risk to build impact of the most extreme processing conditions.

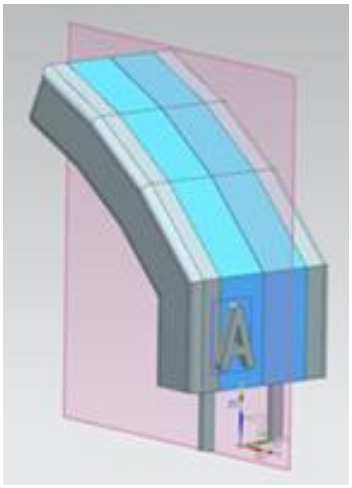

***Figure 26. Multi-Angled Downskin Sample Providing 45, 35, and 25-Degree Downskin with Stitch Width Highlighted in Blue***

The geometry was also designed for characterization mounting, with a cut-plane along the red plane shown in Figure 26, and flat overhang regions to facilitate consistent surface roughness measurements. After printing, each sample had the three individual angles measured under a Keyence light microscope, providing a topology map of the surface. The DOE space was designed to explore shear, gap and overlap misalignment errors, while holding additional stitch variables constant. Two downskin parameters were applied to the part; an initial downskin optimized for the 45-degree build condition was applied to both 45 and 35-degree overhangs, while a lower energy density parameter was applied to the 25-degree overhang.

*Build Analysis*

When assessing the stitch region of a downskin, the first area for consideration was the surface finish response with a stitch application and no level of optic train misalignment. Investigating the surface finish behavior of the downskin when applying overlapping stitch strikes in the build region, increasing the total amount of processing in the downskin region, potentially causing a change in behavior. Figure 27 shows the comparison between the two conditions, with resulting surface finish values showing no discernable difference between the two for any of the angles investigated. This highlights the potential resilience of the downskin region for low level misalignment build conditions due to the optimized parameters towards optic train misalignment.

Each downskin angle can be assessed both visually and through surface finish measurements against increasingly large amount of simulated optic train misalignment. Figure 28 illustrates the 45-degree downskin surface with increasing levels of shear and gap/overlap misalignment. The process shows greater resilience to the gap/overlap misalignment condition in comparison to the shear type and illustrates the type of surface finish condition that larger misalignments showcase. As the misalignment increases, larger meltback regions begin to appear, showing intermittent unstable melt pool regions that form along the surface.

To assess the change in surface finish behavior, each angled surface was normalized against the no-stitch downskin condition. In addition, the vertical surface measured from the same parts

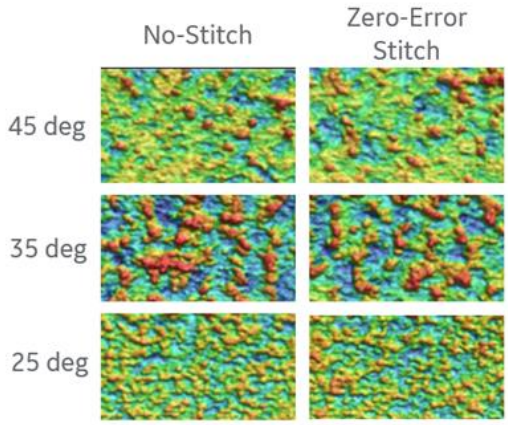


***Figure 27. Downskin Regions without Stitch (left) and with Perfectly Aligned Stitch (right)***

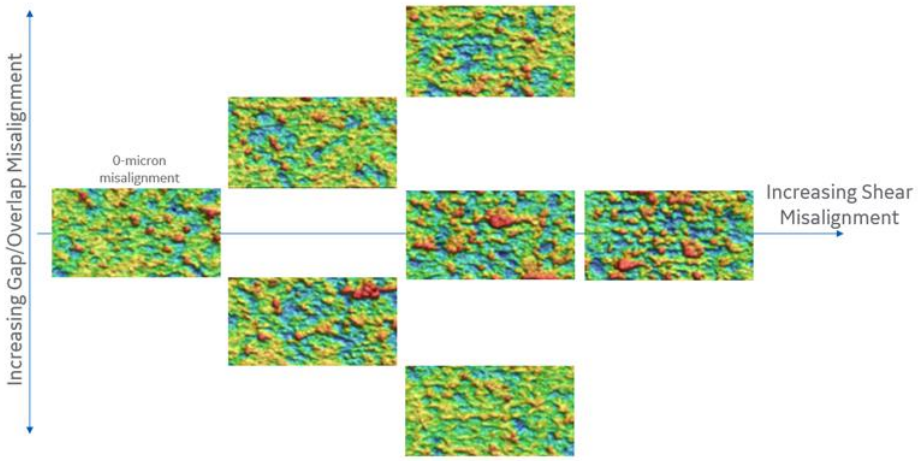


***Figure 28. Surface Topology Maps of 45-Degree Downskin with Increasing Levels of Optic Train Misalignment***

was added to the analysis, acting as a baseline feature. When mapped against increasing levels of misalignment, as shown in Figure 29, an apparent trend was immediately visible. The vertical surface shows an immediate and steady increase as the optic train misalignment in the system increases. This follows a similar trend found with the tortuosity measurements from the vertical thin wall samples. In contrast, the downskin regions are far more stable throughout all misalignment levels, in relation to their no-stitch surface finish conditions.

When the vertical surface was removed from the plot, Figure 30, more variability is shown with the downskin angled regions, though to a much smaller magnitude of relative change versus the vertical condition. Across all three angles, a trend was found where the surface roughness increased significantly only in the more extreme half of the misalignment amount. This led to the original assumption of downskin surfaces, that the parameter set was better able to accommodate an amount of optic train misalignment through better thermal management than a parameter optimized for more vertical and stable build conditions. The same processing space and resulting melt pool formation would not be directly transferrable to vertical orientations due to changes in the processing and thermal boundary conditions of the part but provided a solution for more extreme build conditions.

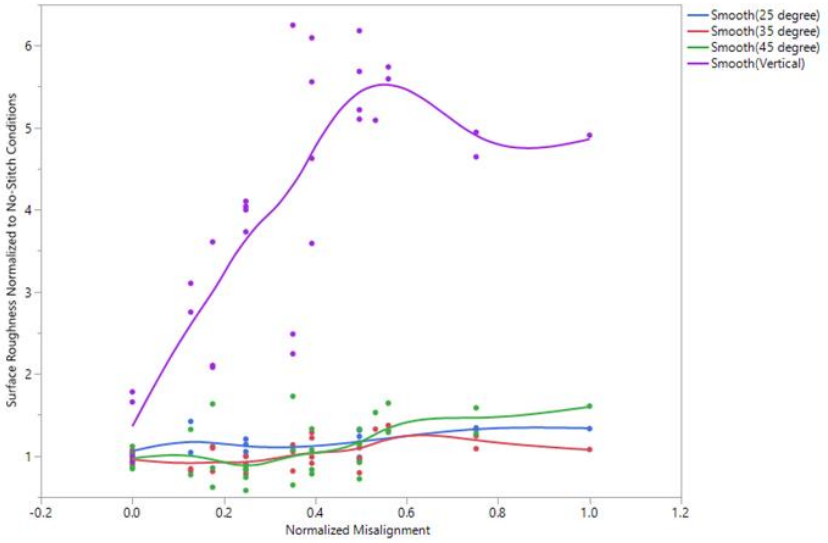


***Figure 29. Downskin Surface Roughness versus Optic Train Misalignment***

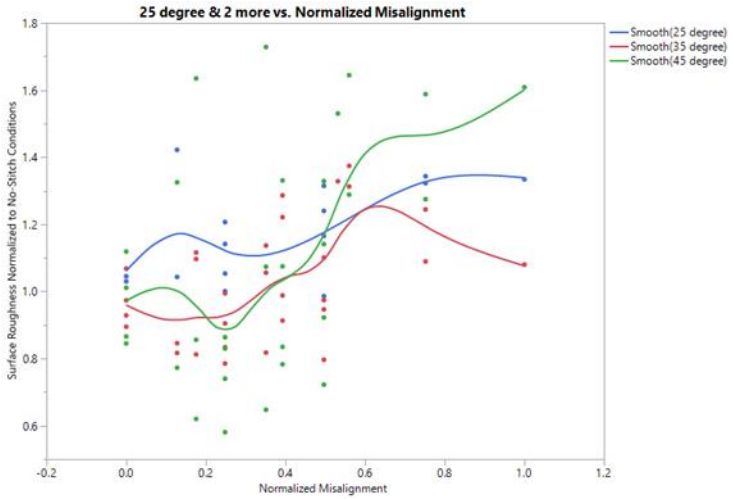


***Figure 30. Downskin Surface Roughness versus Optic Train Misalignment, without Vertical Feature***

*Conclusions*

Multi-laser additive stitching is a novel technology area that adds new capabilities and parameters to the additive process, providing a path to higher throughput and large-part enablement. The key driver for this effort was the exploration and characterization of stitch behavior with the additive process across common features that may be susceptible to two-laser operation. The thin wall feature, down to a 0.5mm wall thickness, is influenced both with material void formation and surface finish. The surface finish of the part is impacted by the amount of shear optical train error and the orientation of the stitch line relative to gas flow direction, though it can be mitigated through tailored stitch layer-based migration strategies. Thin wall material void formation was found to increase versus its no-stitch method as the wall thickness reached 1mm and thinner wall thickness. Creating an increasing likelihood of void formation as higher optic train misalignment is introduced during part processing. This highlights a deviation in stitch robustness between thick walls on the order of 3mm and thin walls of 1mm, with thicker walls being less susceptible to stitch misalignment. One potential impactful stitch parameter to mitigate this formation is the stitch width, the within-plane region that the stitch can migrate between across successive layers, with a larger width reducing the void formation. Stitched overhangs prove to be a more robust geometric feature, with surface finish being impacted at more severe levels of optic train misalignment, relative to already realized increases in surface roughness found in single laser conditions.

The findings from this project highlight key additive feature metrics influenced through the introduction of multi-laser stitching, and potential mitigation strategies through the use of existing features detailing how a stitch is introduced to the part. Moreover, it provides a path to accelerate future findings, provides context to the stitch formation and acts as a reference set of data as stitching is introduced to increasingly complex parts and geometric features.

#### 3.2.2.3 Melt Pool Sensor Stitching Assessment

The purpose of this effort was to evaluate the feasibility of existing model-based statistical process control (SPC) in stitch regions. In a simulated stitch test build with controlled offset between scan lines on each side of the part, the team was able to observe a small shift in the stitch region that varied with offset. This effect was successfully modeled with model residuals in the stitch region indistinguishable from those in the rest of the build. This provided evidence for the feasibility of this SPC approach going

forward as work continues to establish a fixed process and define tolerances relative to alignment and other stitch related variables.

*Goals/Outcomes*

As stitching capability matures into production, ensuring the repeatability and quality of the stitch region will be critical. Melt pool monitoring is expected to be important to SPC to monitor process stability and ultimately significant part of the overall quality process. The aim of this work was to assess feasibility and identify barriers related to the current GE approach to melt pool monitoring based SPC for stitch regions.

SPC with regard to melt pool monitoring is used to identify when, during a production build, process conditions deviate from a known good, qualified process. As with any SPC, implementation takes place in two phases. In the first phase, normal process variation or common cause variation is characterized while the second phase monitors the production process for special cause variation that indicates some change from normal process conditions. Melt pool emissions vary normally as a function of part geometry and a variety of scan path parameters. As such, a critical part of Phase 1 SPC for melt pool monitoring involved training a model and characterizing the normal deviations from this model. The degree to which the model quantitatively describes the normal process variation provides the primary limitation on process shifts that can be detected. A fixed, stable process was a prerequisite to advancing to Stage 2. The current stitching process is still under development and it is therefore not realistic to develop the full SPC process and limits. The focus of this effort, in the absence of a finalized, fixed stitch parameter set, was on assessing the current capability to create a process model that describes the stitch region. A simulated stitch build would be used to this effect to achieve two primary goals:

1. Qualitatively assess changes in the melt pool emission signal in the stitch region of a test coupon
2. Create and evaluate a melt pool model to determine feasibility of the current model-based SPC approach for stitch region evaluation

If the current model features fail to describe the stitch region sufficiently, new model features would be proposed and evaluated. It is expected that as stitching technology matures and the team converge on a final stitch parameter set, model features will need some degree of tuning and adjustment. The expected outcome of this work was to ensure that only tuning of the model would be needed with no fundamental change in the model features or methodology when stitch parameters were finalized.

*Melt Pool Monitoring and SPC*

The QM melt pool system on the Concept M2 machines was used for this work. It is essentially identical to that used on the Mline machine and thus serves as a good model for the larger machine platform. A simplified diagram of that system is shown in Figure 31 for a single laser. The system consists of two sensors, infrared (IR) avalanche photodiode and a visual camera. These are arranged in a downbeam or on-axis configuration such that the field of view of each is centered at the laser focal point and follows the laser scan path. From an analytics perspective, the camera was not being used at this time but could be used to provide additional resolution into process conditions in the future. The photodiode does not give an absolute temperature value but does provide a useful and valuable measure of the thermal energy in the melt pool. The photodiode and related sensor optics are sensitive to IR light emitted from the melt pool in a relatively narrow band below the laser wavelength. IR light reaching the photodiode is converted into a voltage which is monitored in a data acquisition system. As melt temperature increases, so does the intensity of the IR light emitted in that narrow band and

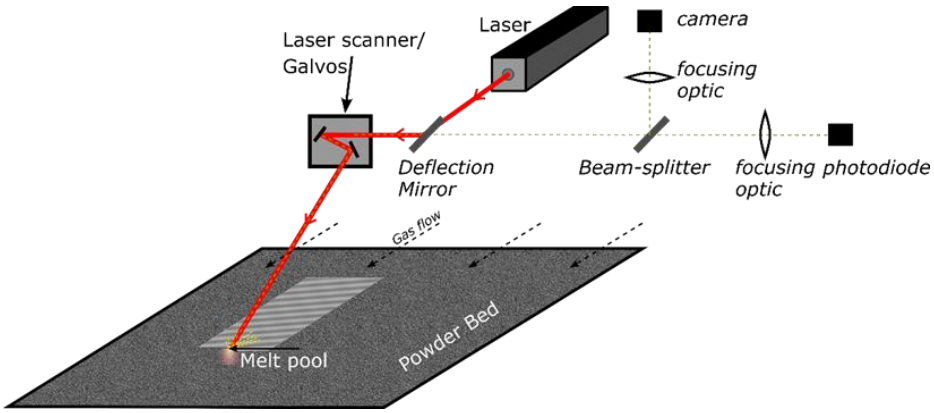


***Figure 31. QM Melt Pool System Illustration***

consequently, the voltage output from the photodiode.

Melt pool temperature and hence measured photodiode response are not constant during a typical additive build process or even across a given layer of a build. A degree of variation in the photodiode response can be attributed to the optical system through which the emitted IR light must pass. This is readily corrected through a calibration process. Further variation is associated with scan path parameters and part geometry with a complex multivariate dependence observed. While many important scan parameters are controlled such as laser power and scan speed, others inherently vary throughout the build, such as scan direction and incidence angle. Above the melt pool is typically a cloud of vaporized material, spattered particles, and often a plasma. This is apparent visibly in the form of sparks or a "comet tail" emanating upward from the melt pool shown in Figure 32. The direction of this tail is a function of the scan direction, scan speed, and gas flow velocity. Material in the "comet tail" can interact with IR light emitted from the melt pool, reducing the observed photodiode signal. This is one of several scan path related phenomena impacting the observed melt pool signal.

To enable SPC, a multivariate machine learning algorithm is used to create a reduced variable set from which a model of the photodiode response as a function of scan path and thermal conductive properties associated with the part geometry. Control charts are created based on the difference between the measured and predicted photodiode response. The ability to resolve process shifts with this approach is limited by the fidelity of the melt pool model. Stitching regions may be expected to exhibit different melt pool behavior from the rest of the part during an additive build process. In the stitch region, laser scans transition from powder to previously scanned, solid metal, inherently altering the nature of the laser-material interaction. Retained heat from the first laser pass and alignment of the scan lines from the first and second lasers may also impact the resulting melt behavior and consequent observed photodiode response. This presents a potential risk in applying the current model-based SPC approach to stitched regions. Assessing and mitigating this risk was an expected outcome of this work.

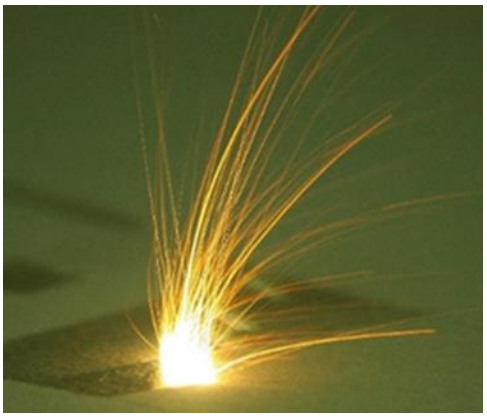

***Figure 32. Sparks Emanating from Melt Pool in Form of "Comet Tail"***

*Test Build*

A test build was designed to simulate stitching on a Concept M2 machine. The test component, a "jailhouse" part, consisted of a solid base with an array of thin walls of variable thickness and a solid top, as illustrated in Figure 33. Either side of the part was scanned separately to simulate stitching with a single laser. By using a single laser, alignment or misalignment between the laser scans on either side of the part could be controlled. Best practices for maintaining alignment of scan fields from multiple lasers is still under development. The build layout consisted of 64 parts, as shown in Figure 34, with misalignment ranging from 0 to 70 µm. This represents what it expected to be the same order of magnitude of misalignment that might be reasonably expected once tolerances and alignment procedures are finalized.

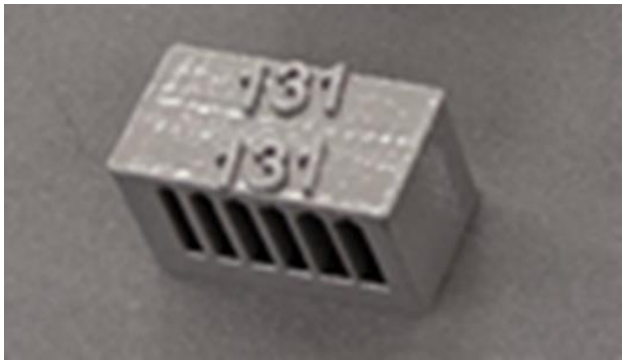

***Figure 33. Example of "Jailhouse" Part Used for Stitching Assessment***

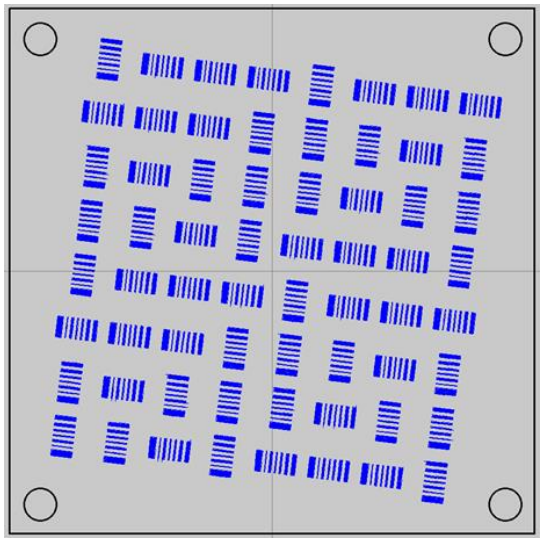

***Figure 34. Jailhouse Build Layout of 64 Parts on Build Plate***

*Data Assessment*

An initial assessment of the melt pool data indicates a shift in the photodiode signal corresponding to the location of the stitching zones. Figure 35 illustrates this for Layer 50 in the solid base region of the build. Insets show details of a single test coupon and again of the stitching region itself. The typical shift was observed to be on the order of ~10% from the bulk melt pool signal. For the part highlighted, the bottom half of the part was scanned first, as shown by the timestamp data in Figure 36. As shown in Figure 37, a similar scenario was observed in the thin wall region.

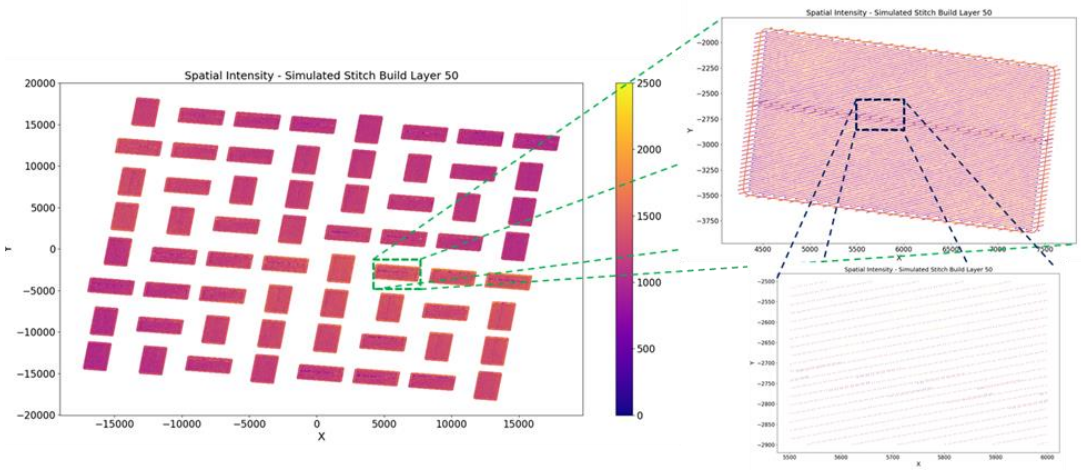


***Figure 35. Photodiode Intensity for Layer 50 of Test Build with Insets Showing Details of Individual Part***
*A reduced photodiode signal is observed in the stitching region*

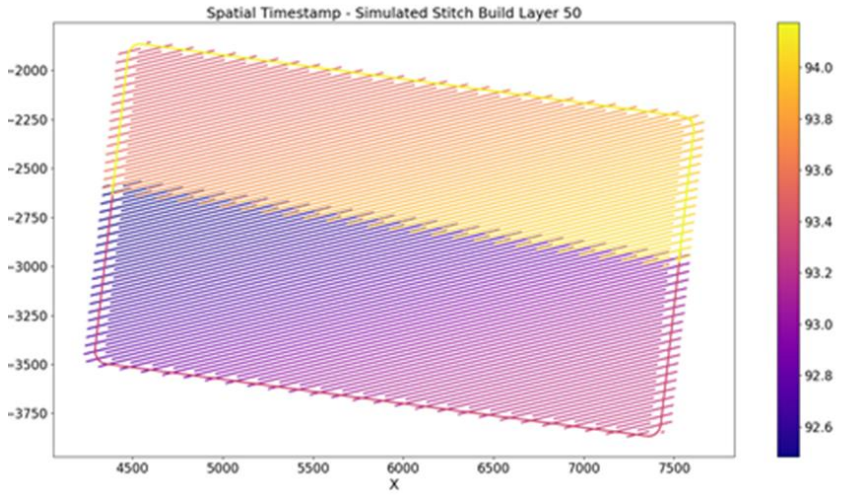


***Figure 36. Time Stamp for Photodiode Data of Part Highlighted in Figure 35***
*The bottom half is scanned first followed by the top which overlaps in the stitch region in the middle*

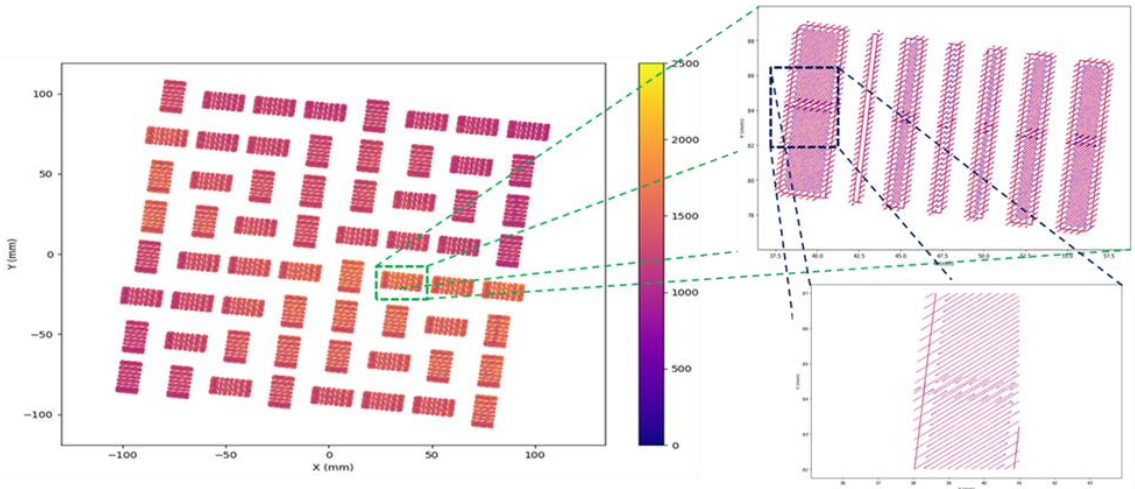


***Figure 37. Photodiode Intensity for Layer 104 of Test Build with Insets Showing Details of Individual Part in Thin Wall Region***
*A reduced photodiode signal is observed in stitching region*

While not readily apparent in the previous figures, the offset between the scan lines was observed to have a small but significant impact on the photodiode signal from the melt pool. As noted previously, offset between the laser scan lines on either side of the stitch region varied from 0 to 70 µm. This offset can be observed in the photodiode spatial data map, as illustrated in Figure 38. The photodiode intensity on average decreased slightly, by ~100 counts, as offset was increased to its maximum value. This is exemplified in Figure 39 and Figure 40 showing representative single laser strikes and full part layers. Gaps in the data represent times when the laser was off or scanning elsewhere in the build. In each part, a first small gap was observed as the laser shifts from the bulk scan to the contour scan then a large gap before commencing bulk scanning on the other side of the part. This was followed by another smaller gap before the contour of the second side of the part was scanned. The small, but significant differences between the two cases was an indication that the photodiode signal could be used as an indicator of scan field misalignment. The same data is shown spatially in Figure 41.

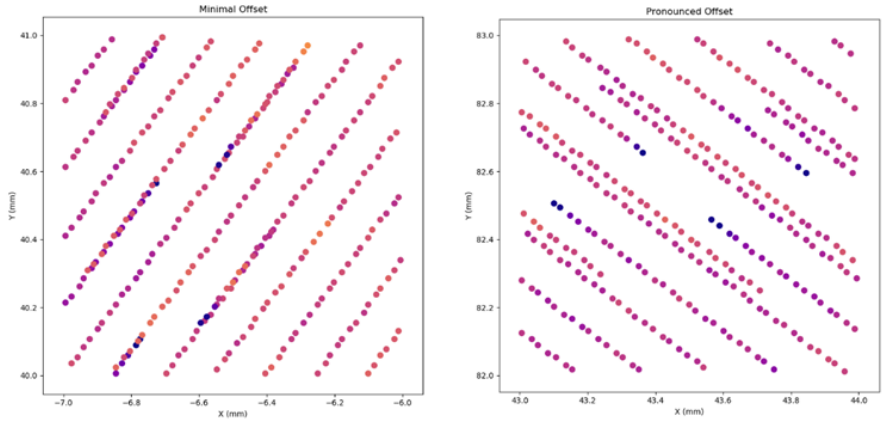


*Figure 38. Offset Between Stitch Lines Illustrated in Photodiode Data Map*

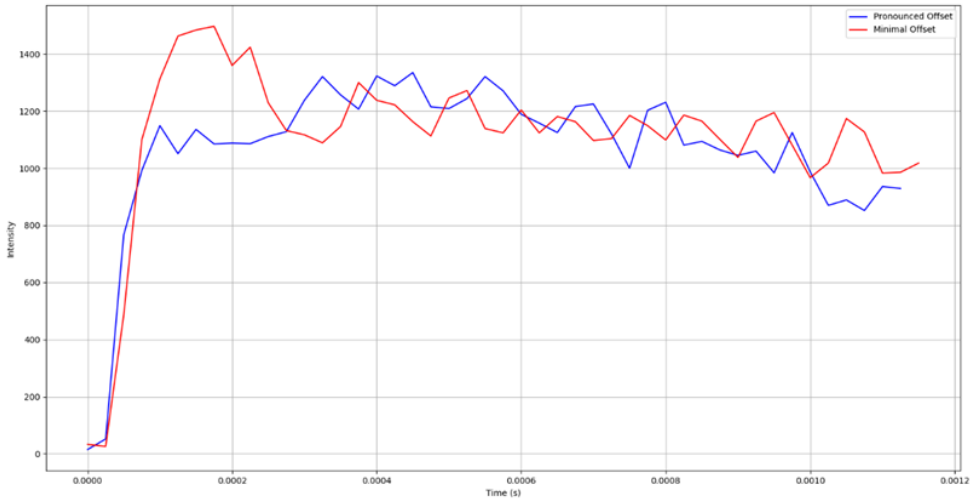


*Figure 39. Photodiode Intensity for Single Laser Strike in Stitch Region with No Offset and Maximum Offset*

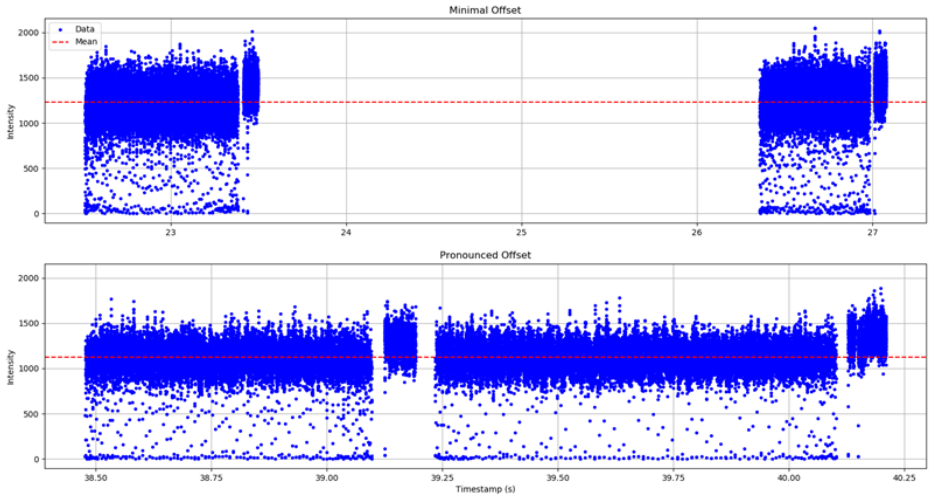


*Figure 40. Comparison of Time Series Photodiode Data for One Layer in Base Region with No Offset and Maximum Offset Between Stitch Scan on Either Side*

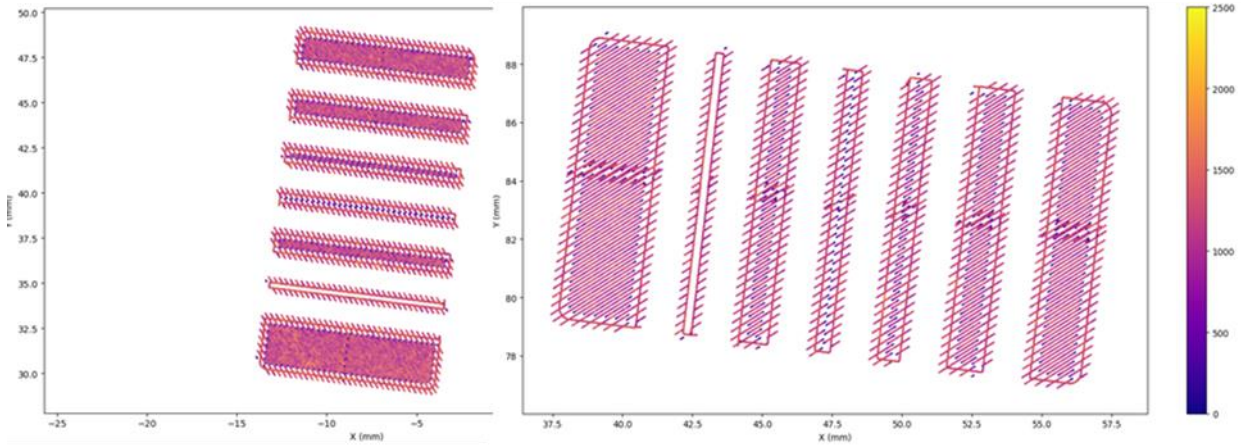


***Figure 41. Comparison of Stitch Region Shift in Stitch Region of Thin Walls for Parts with No Offset (left) and Maximum Offset (right) in Spatial Domain***

The relatively small shift in the stitch region provides confidence that this region can be treated as part of the same data population in a model. For production, a model would need to be trained from a population of multiple builds and machines to capture build-to-build and machine-to-machine variation respectively. As a feasibility assessment, a model was trained from a small sample of the data from the test "jailhouse" build and applied to the remainder of the build. The varying offsets were treated as normal variation in the process and no attempt was made to distinguish between the high and low/no offset conditions. Once a maximum allowable offset was defined, data from any builds or parts exceeding that maximum would be excluded from the training population.

*Conclusions*

The primary purpose of this effort was to evaluate the model-based SPC approach for melt pool emissions in stitching regions. A simple test stitch build was performed and melt pool signals qualitatively evaluated. Small shifts were detected in the stitch regions with a dependence on the alignment between scan lines on either side of the stitch region also observed. A model was trained using a small fraction of the data from this build and applied to the remainder of the build. The fidelity of this model was comparable to that observed in previous efforts with no apparent difference observed between residuals in the stitch region and the rest of the build, providing confidence in the feasibility of this approach moving forward. Additional work will be needed to evaluate time lag effects between either side of the stitch region, which is being pursued in a separate effort with promising results. Once a fixed process is defined, a model can be developed with a larger population and control limits established and compared to process tolerance limits.

## 3.2.3 Task 2 – DDM Plan Development

### 3.2.3.1 VSE/SPS Plan Development

The VSE/SPS efforts were completed during this final phase of the program. As part of these efforts, the determination of the final part post-printing requirements involved reviewing the processes for the current production part (6053T29) which were then assessed for applicability to the new additive part. These included FPI, pressure check, cleanliness, as well as several others. Additional requirements specific to the AM process were also identified. These items formed the basis for the VSE/SPS requirements for the final Additive Swirl Frame part developed under this project.

An overview of the VSE/SPS processing workflow for the final Additive Swirl Frame part is shown in Figure 42.

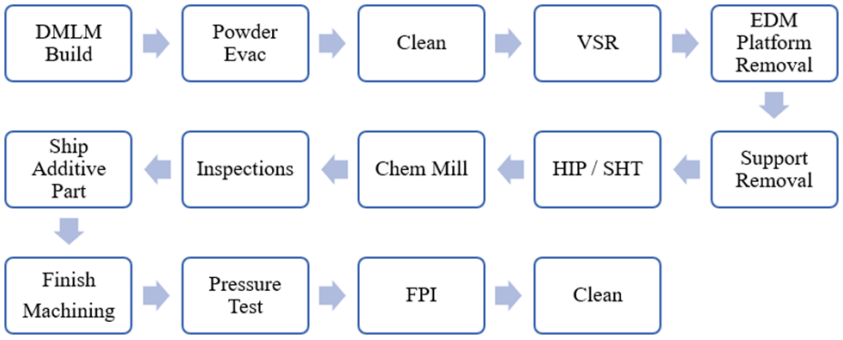


*Figure 42. Flowchart of VSE/SPS Steps*

Each of these steps shown above were included to ensure that the finished part meets design intent.

#### 3.2.3.2 Industrialization Studies – Component Build Development

The two full part builds that were completed under the previous Phase 2 contract were completed using an EOS machine. However, these were no longer available as GE had transitioned to Concept Laser products. Consequently, all builds completed in this CTMA project (for Phase 3 and 4) were performed using the GE ATLAS machine. An overview of the ATLAS 1.1 machine is shown in Figure 43.

This large format machine has been operational in a beta format since 2017 and has well over 10,000 hours of operation on multiple serial numbers and at multiple user sites. The key to ATLAS' success lies in its unique approach to laser powder-bed fusion. Unlike most powder-bed machines; the build plate is fixed, and a gantry translates the scanner and contained gas flow over top of the plate. This allows for large-scale additive prints without sacrificing fine feature resolution or material properties.

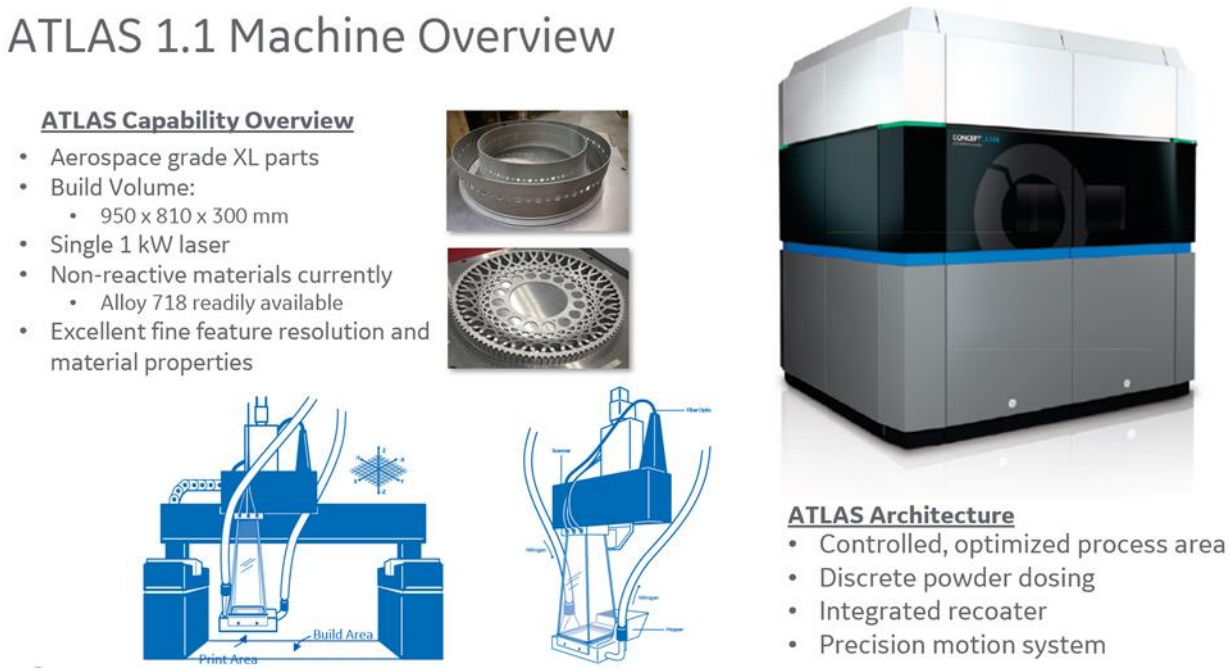


*Figure 43. ATLAS 1.1 Overview*

After initial success with the ATLAS 1.1 machine, the platform was upgraded to improve safety, process, and productivity. The upgraded version of the machine is called ATLAS 1.2. The ATLAS 1.2 boasts improved gas flow consistency and soot clearing abilities, additional filter life with reduced build interruptions, a new plate fixturing method that allows for part distortion that is typical with the residual stresses produced by larger format parts and other modification to improve machine error handling and sensing control. An overview of version 1.2 is shown in Figure 44.

**ATLAS Initial Printing (Build #1)**

Building on the success of the second full part build (see Figure 45) which was successfully completed in late 2017 as part of the Phase 2 contract, the third full part printing was initiated in December 2019 using the ATLAS 1.2 machine with Inco 718 powder. This build is denotated as ATLAS Build #1. All subsequent builds completed for this program will be referred to as ATLAS Build #. ATLAS standard 235W parameters were utilized with a 50 µm layer thickness. As noted in Section 3.2.4.1, the wall thickness of the vanes in the initial build were 0.040". This vane wall thickness was the same as all previous builds but is thicker than the current production part vane wall thickness of 0.020". The increased thickness was chosen to ensure successful additive builds.

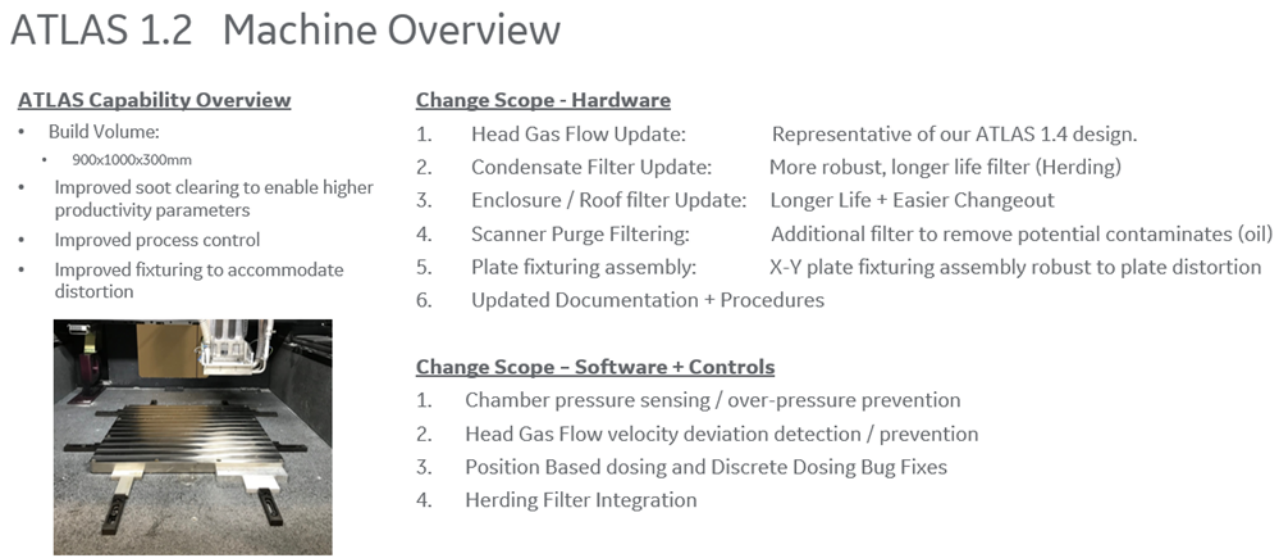


***Figure 44. ATLAS 1.2 Overview***

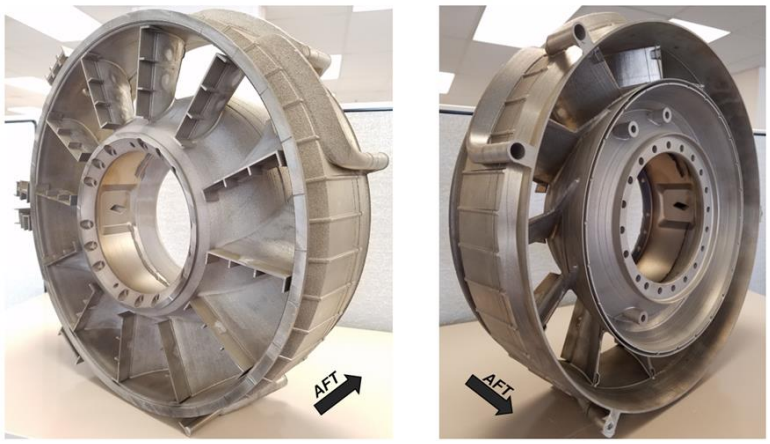


***Figure 45. Phase 2 Contract – 2017 EOS Machine Full Park Build #2***

The first ATLAS build was successful with no anomalies noted. Figure 46 shows the completed printing of the 0.040" vane wall Swirl Frame which will be referred to as ATLAS Build #1.

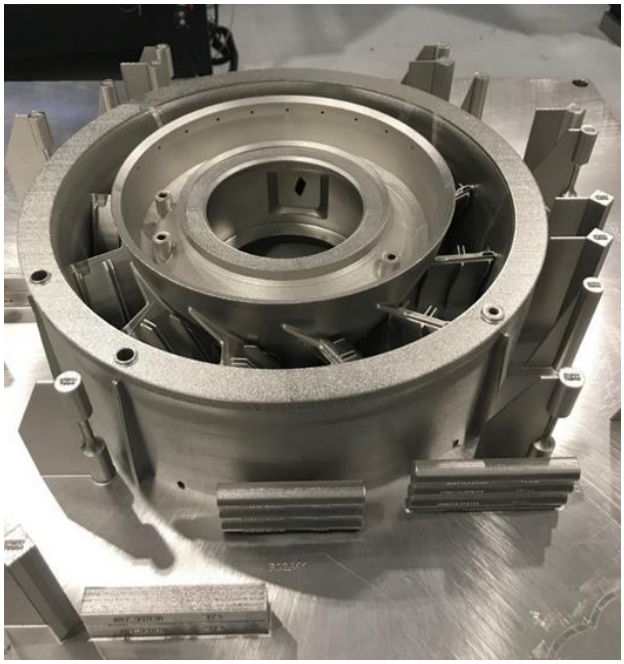

*Figure 46. Initial Print on ATLAS Platform with 0.040" Vane Wall Thickness (ATLAS Build #1)*

**ATLAS Build #2 Summary**

Following the successful completion of the ATLAS Build #1, a second build was initiated. For this second ATLAS build the vane thicknesses were reduced to 0.20" thickness to match the current production part. Unfortunately, ATLAS Build #2 failed on Layer 2437 of 3223 (121.8mm build height) after 306 hours of continuous operation. The build experienced gross powder-bed disturbance across the entire powder-bed. A root cause investigation determined that an adjustment to the outer diameter flange support resulted in an under supported overhang.

**ATLAS Build #3**

As noted in Section 3.2.4.1, to address the root cause of the ATLAS Build #2 failure, ATLAS Build #3 modified the outside diameter flange support structure to be full height. Additionally, as detailed in Section 3.2.4.1, the vane wall thickness was reduced to 0.030". The build was initiated and was proceeding well until around Layer 1600 (80mm build height). At this layer, two areas on the build started to cyclically peel up and heal over a roughly four-hour period. At Layer 1649 (82.4mm build height) the build was paused after a small delamination did not heal and peeled away from the powder-bed, creating a risk of recoater damage.

The build chamber was opened during the build pause at layer L649. The small area of delamination was clipped, removed, the surface lightly filed down to eliminate any powder-bed protrusion and the recoater blade replaced. The build was re-started with the intent to finish the build and identify any other areas of concern with the part model. The build finished successfully after this intervention. No additional areas of concern were identified. The final build condition is shown in Figure 47.

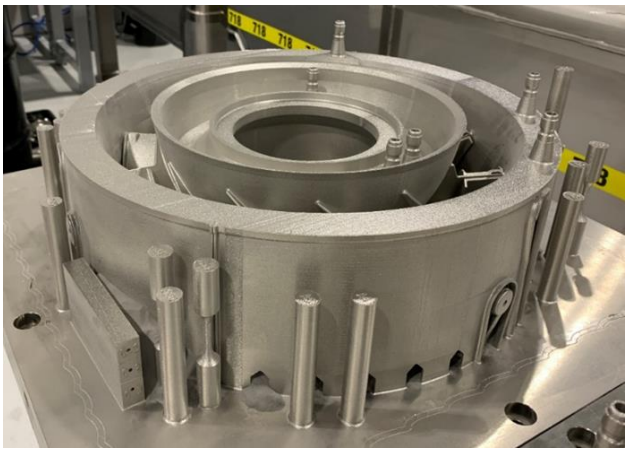

*Figure 47. ATLAS Build #3 After Bulk Powder Removal*

**ATLAS Build #4**

To address the issues experienced in ATLAS Build #3, the support structure ring diameter was increased to reduce interference with part features and the unsupported radii locations mentioned above were modified. Details of the changes can be found in Section 3.2.4.1.

ATLAS Build #4 completed successfully with a final print time of 394.5 hours. This build, like all previous iterations, utilized ATLAS standard parameters (235W) with a 50 µm layer

thickness. A single machine anomaly occurred at Layer 38 where a powder feed error was noticed. The machine automatically paused after detecting this error and technicians were able to address the issue upon finding the error. The build was paused for a total of 14.6 hours. The anomaly occurred in the stock on upper region of the part, and it was deemed acceptable to continue the printing operation. Standard ATLAS re-start procedures were followed when re-starting the build.

No additional build stops, or machine anomalies occurred during the duration of the print. Upon printing completion, the bulk powder was removed. A photo of the part in the as-printed state prior to build plate removal is shown in Figure 48. This part met all as-printed additive casting requirements, was released to the follow-on post-processing steps detailed per the VSE/SPS detailed in Section 3.2.3.1 and officially was assigned as the final single lot program deliverable.

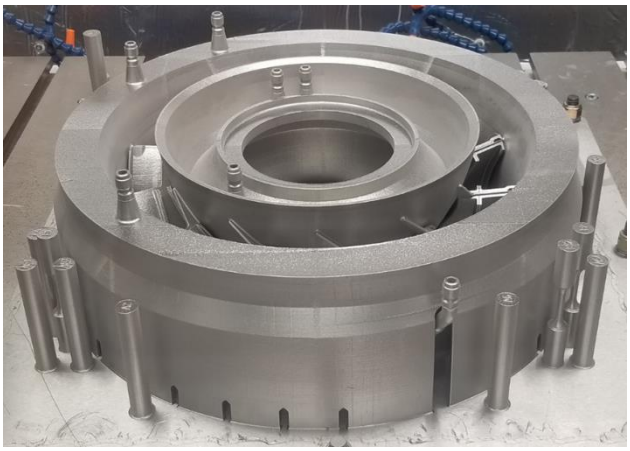

***Figure 48. Build #4, Post-Powder Removal***

## 3.2.4 Task 3 – Engineering Validation

### 3.2.4.1 Additive Build Model Modification

As detailed in the Phase 3-4 progress report, the production model/drawing for the Additive Swirl Frame utilizes a three-tier approach that includes an additive print model with support structure, an additive model without support structure (or additive casting) and a final machining model/drawing.

Leveraging the successful EOS Machine Full Part Build #2 completed in 2017 as part of the Phase 2 contract, the first ATLAS build (ATLAS Build #1), utilized a 360-degree support structure around the aft flange of the part which spanned the full build height. This support structure included breaks in the structure for interfering features but still provided the necessary build support. Water wash and anti-ice holes were printed open in this build but closed in later iterations as they posed a challenge for sealing passages during chemical milling.

ATLAS Build #1 also utilized the successful vane support structure demonstrated in the successful Phase 2 builds. The vane wall thickness for this build was 0.040” which was the same wall thickness as the previous full part builds. For reference, the current production part utilizes a 0.020” vane wall thickness. The details of the build process are discussed in Section 3.2.3.2.

The next full part print, ATLAS Build #2, took a different support structure approach. In this build the aft flange, was supported by a ring of material under the flange with arched shape cut-outs that bridged between the flange and the cylindrical main body of the Swirl Frame. This support structure concept was implemented to reduce overall print time and powder usage. Unfortunately, this support structure proved to be inadequate for supporting the overhang of the aft flange and the print failed in this region. This build failure is detailed in Section 3.2.3.2. All subsequent builds utilized a full support ring that spanned from the aft flange to the print bed, similar to the support structure of ATLAS Build #1 discussed above.

Based on the build issue encountered in ATLAS Build #2, the third full part print utilized a 360-degree support structure around the aft flange of the part that spanned the full build height of the

part. However, for ATLAS Build #3, print time reducing features were incorporated at the base of the support ring. The anti-ice and water wash holes that were printed open in ATLAS Build #1 were closed in this build and were opened during final machining. Flight Counter support brackets were added to the printed part to eliminate the need for brazing and to further reduce overall part count. Additionally, quick connect geometries were added to all part features that opened to internal passages. These quick connections features mate easily with fixtures used during the powder removal and cleaning processes to reduce the time required to complete these tasks.

A significant change incorporated in the ATLAS Build #3 CAD model was a reduction in the vane wall thickness from 0.040" to 0.030". This reduced printed wall thickness in combination with a post-print chemical milling material removal delivered the same 0.020" vane wall thickness as the production part (6053T29). The vane support structure utilized in ATLAS Build #3 was the same as that of ATLAS Build #1.

The fourth and final full part print on the ATLAS utilized a similar support structure ring as ATLAS Build #3 with the diameter of the support ring increased to reduce interference with part features. This reduced the number of required close-outs within the support structure, lowering the risk of print failure. The vane wall thickness and vane support structure were the same as those of ATLAS Build #3.

#### 3.2.4.2 Dimensional Capability Studies

Before initiating the final machining, a 3D scan was taken of the additive casting of the ATLAS Build #4 part. The results of the scan were then best fit inside the additive casting CAD model used for the printing. A positive dimension indicated that the scanned part was outside of the nominal model or had a stock-on condition. A negative dimension indicated that the scanned part was inside of the nominal model or had a stock-off condition. The color scale shown in Figure 49 and Figure 50 ranges from negative, pink, stock-off to positive (red, stock-on). It should be noted that due to program constraints and requirements no pre-printing geometry compensation was performed which is typical of production programs.

Figure 49 shows an aft side view of ATLAS Build #4 best-fit in the nominal CAD model. This information was used during the final machining process to determine where to

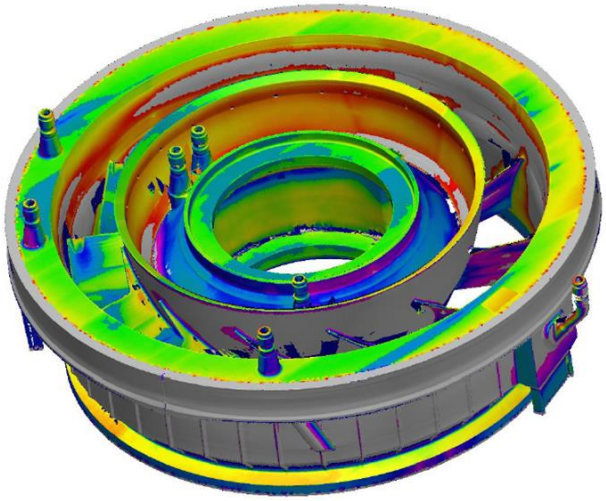

***Figure 49. Deviations from ATLAS Build #4 to CAD Model, Aft Side View***

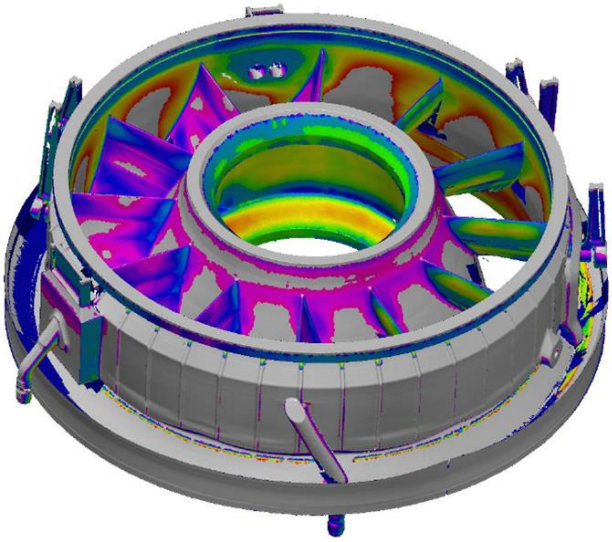

***Figure 50. Deviation from ATLAS Build #4 to CAD Model, Fwd Side View***

machine all finished surfaces within the additive casting to best meet the finished part drawing definition. Figure 50 shows a similar deviation map with a forward side view of the part.

The most significant deviations shown in Figure 50 occurred on the vane faces. Because these were not machined surfaces, and due to the scope of this project, these deviations present on the finished additive part. If this part were taken to production these deviations would be pre-compensated for in the additive print CAD model to mitigate these issues.

## 3.2.5 Task 4 – Industrialization Efforts

### 3.2.5.1 Final Machining Drawing

As detailed in the final report for Phase 1 & 2 of the program, significant part count reduction was incorporated into the design of the Swirl Frame as enabled by the use of DMLM printing. In addition to these modifications several other part features were also modified, combined, or added to the final part CAD model as the design team learned from each successive additive build. One of these added items were the Flight Counter attachment brackets. In Figure 51, the Flight Counter mounting brackets are shown on the current Production Swirl Frame (6053T29) (Note: additional un-related instrumentation is also shown on the part).

In the production configuration the brackets are brazed onto the outer wall of the Swirl Frame and nut plates are then riveted to each of the brackets (which can be seen in Figure 51). In the additive part these brackets, shown in Figure 52, are integral to the part, further reducing part count and assembly operations. Key-locked threaded inserts are used in place of nut plates in this instance to prevent thread damage to the base part.

The threaded inserts allow for the same functionality as the nut plates. Similar threaded inserts are used on the production hardware in the T2 sensor boss and in the anti-ice boss. The Additive Swirl Frame also uses threaded inserts at these same locations as shown in Figure 53.

*Figure 51. Flight Counter Mounting Brackets on Production Swirl Frame (6053T29)*

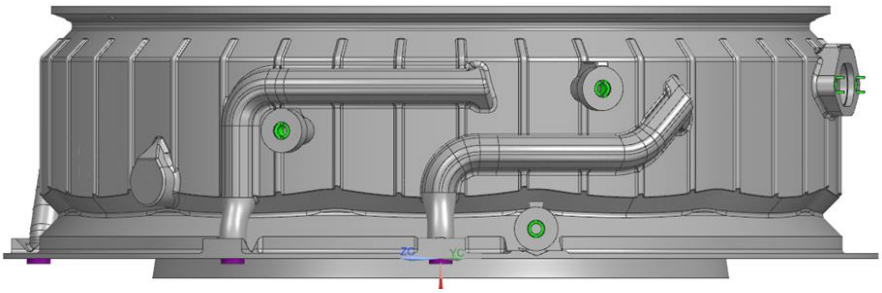

*Figure 52. Flight Counter Mounting Brackets with Inserts on Additive Swirl Frame*

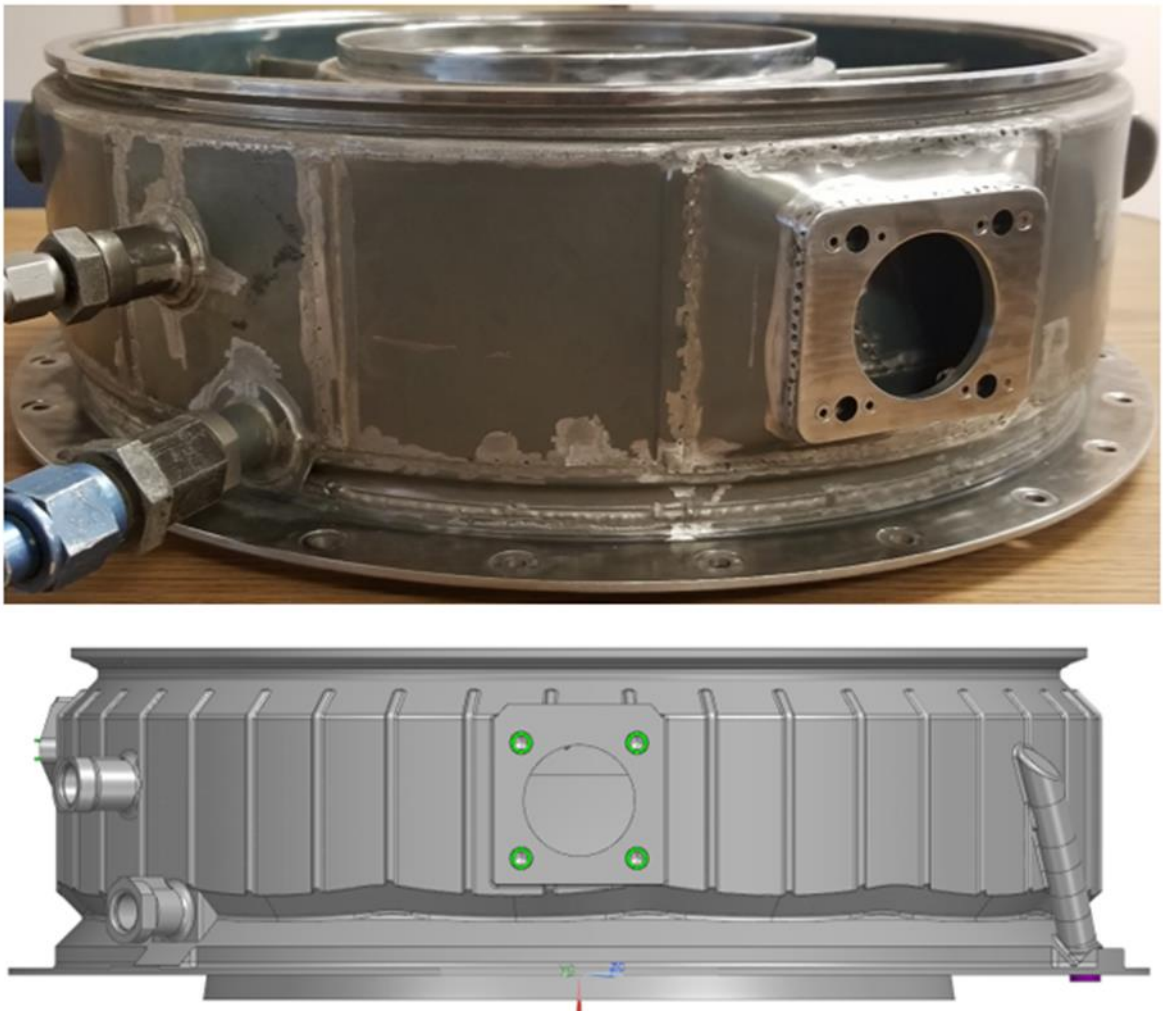

*Figure 53. Anti-Ice Boss on Production (6053T29) (top) Additive (bottom) Swirl Frame*

### 3.2.5.2 Single Lot Final Part Production

The final single part program deliverable was produced from the ATLAS Build #4 additive casting described above in Section 3.2.3.2 as well as in Section 3.2.4.1. The final part was processed following the VSE/SPS plan detailed in Figure 42 which is summarized here again. First, the additive casting was built using the ATLAS machine in this case. Following the printing the part was removed from the machine and sent for powder removal, and then vacuum stress relief. Next, the build platform and build support structures were removed. Following this the part was sent for HIP and solution heat treat. After these steps the part is ready for chemical milling. Chemical milling is the process of using baths of temperature-regulated etching chemicals to remove material.

Chemical milling serves two primary functions in the processing of this part. First, the material removal improves the surface finish of the as-printed surfaces. Secondly, in this case it was used to bring the as-printed vane wall thickness from 0.030” as discussed in Section 3.2.4.1, down to a final wall thickness of 0.020”. This approach was taken to achieve the same vane wall thickness as the Production Swirl Frame (6053T29) while reducing the risks associated with printing thin-walled structures.

For this specific part it was determined that prior to chemical milling, openings to all internal passages in the part must be closed off

or "plugged" in order to prevent the etching chemical from entering. Allowing the chemical to enter internal passages creates a risk that the chemical will become trapped and remove more material than intended before it is deactivated, creating the potential for "burn through" where thin walls, such as those in the vanes, are broken through by the milling agent. This plugging of internal passages is not necessarily required in all instances but is determined on a part-by-part basis and as described above determined to be the appropriate course of action for this part.

A photo of the final additive casting part post chemical milling is shown in Figure 54.

The brassy discoloration visible on the part is an artifact of the chemical milling process and does not impact the structural properties of the Swirl Frame. Additionally, most of the discoloration occurs in regions of the part where it was removed during final machining.

The chemical milling on the final part uncovered several locations with surface irregularities that were created during printing. These areas manifested from a localized short feed on the ATLAS machine. Upon investigation, two factors were identified in the creation of a localized short feed condition. Corrective action for this included pre-build inspection of gate flow uniformity along with documentation of lessons learned for future machine iterations.

After reviewing these irregularities with AM weld experts and the Army ManTech team, it was decided that these areas could be repaired via standard additive weld repair procedures. All locations were successfully repaired and after both internal reviews and reviews with the Army ManTech team the repaired part was deemed acceptable for release to final machining.

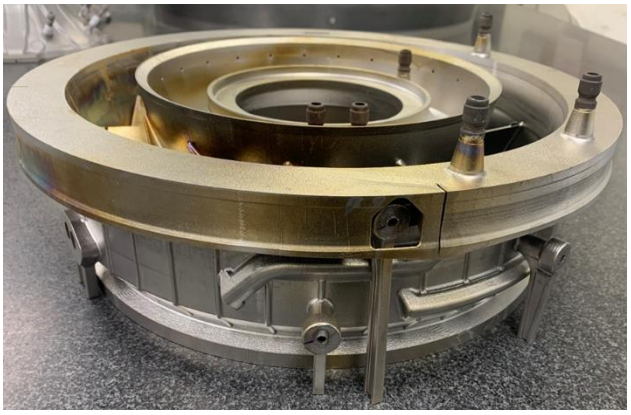

***Figure 54. Single Part Deliverable After Chemical Milling***

As mentioned previously in Section 3.2.4.2, a 3D laser scan was performed by the final machining vendor on the ATLAS Build #4 additive casting before final machining was initiated. The data from this scan was used to create tooling fixtures and tool path programming to ensure final part dimensions could be met. Prior to initiation of the final machining the results of these scans were reviewed and accepted allowing the machining to commence.

During the review of the 3-D scan results of the Build #4 casting and comparison to the actual CAD build file used it was discovered that there was an error in the additive casting build file. Specifically, the water wash port, did not correctly connect with the water wash plenum but instead connected with the anti-ice air outer plenum. The water wash port outlet was closed off from the water wash plenum but was open to the anti-ice plenum. This was opposite to design intent. Unfortunately, as this error occurred inside the part there was no feasible way to repair it other than print a whole new part. After discussions with the Army ManTech team, the decision was made to use this part as-is since the water wash functionality was not required for this demonstration part. To prevent the water wash port from being utilized, the production cap fitting that is installed in this port would be welded in place thereby preventing the water wash port from being utilized.

The final machining of the ATLAS Build #4 additive casting was controlled by drawing 17A206-230. The drawing includes the installation requirements of the threaded inserts and oil passage interface transfer tubes which are the only components from the original production part not additively manufactured. The drawing also controls all interfaces with mating engine hardware and ensures the final additive part will meet all the installation requirements as defined by the current production part. The drawing also details the required pressure and leak testing as well as the FPI and final cleaning of part including the internal oil delivery circuits.

One of the tests required on the production part drawing (6053T29) that was carried over to this part was the pressure and leaking testing of the internal cavities. This covers the water wash, anti-ice, and oil circuits. Based on the intended end use of the final demonstration part it was agreed that only the oil circuits would be tested. All oil circuits passed the required tests.

Similarly, another test that was required on the production part drawing (6053T29) that was carried over to this part was the FPI test requirement. There was a total of six non-conformance locations. One location was on the outer aft flange, which was found to have a flaw outside the 0.060" limit. Additionally, five of the vanes were also found to have flaws outside the 0.060" limit in the outer diameter blend fillet region.

To assess the potential impact of these FPI non-conformances the team looked to the 2013 and 2016 CT7-2E1 FAA Certification reports as these were the most recent and up-to-date stress and life assessment of the Swirl Frame available. Specifically, the team utilized the Chapter 5 Static Structures Cyclic Life Report stress and life analysis assessment as the basis of acceptance for these non-conformances. It should be noted that a CT7-2E1 engine is essentially the commercial equivalent of the T700-701D engine and both engines use the same production Swirl Frame (6053T29G01) that was the focus of this program.

To start with, the operating loads affecting the Swirl Frame stress and life during a given aircraft mission can be characterized as follows (It should be noted that the 2013 certification assessment considered UH-60 Black Hawk loads in their analyzes):

- Thermal-mechanical
- Aircraft maneuver
- Engine torque
- Vibratory (engine and aircraft-induced)

A key thing to note here is that the program required use of the final single lot part delivered under this program is an engine assembly fit check only. If in the future the Army decided to use this asset on a T700 ground test demonstration the loads the Swirl Frame would encounter would be a subset of the above as shown below:

- Thermal-mechanical
- Vibratory (engine only)

This is a very important distinction as the largest loads the Swirl Frame encounters in service are the engine mounting loads and these are not present in a ground test installation due to the differing engine mounting configurations between the aircraft and test cell. A key factor to understand is that the Swirl Frame is structurally considered a combination of a major static structure (Forward Engine Mount) and other static structure. A major static structure in the case of the Swirl Frame means it is part of the engine mounting load path and a failure would be considered a potentially hazardous engine effect. This is an important distinction as the FPI non-conformances highlighted above all occur in the other static structures area and as such are not high risk failure locations and are not considered life limiting locations. It also bears repeating that in the case of a standard ground test installation the Swirl Frame is not part of the engine mounting load path.

In support of the CT7-2E1 FAA Certification referenced above, 2D & 3D thermal analyses as well as 2D & 3D stress analyses were performed using a mix of loading conditions from the operating environment of the engine. Vibratory analyses were also performed to provide additional boundary conditions for these analyses.

Based on the worst-case cyclic life analysis performed in support of the aforementioned CT7-2E1 Certification, all Swirl Frame critical locations have lives greater than 100,100 cycles Ni (crack initiation). Based on these CT7-2E1 FAA Certification assessments as applied to the FPI non-conformance locations, the Army ManTech team agreed the final single lot production part was acceptable as is. These locations have no impact on the program required fitment check-out. Additionally, these locations would constitute very low risk for any potential future ground test demonstration as detailed above.

The last operation performed on the part prior to final dimensional inspections was the cleaning as defined in the 17A206-230 drawing. The cleaning was done to the same specification as the current production part. This cleaning applied to all areas of the part with special pos-cleaning debris limits on the oil passages. In the case of this final single lot deliverable Swirl Frame, it was cleaned a total of three full cleaning cycles, but the post-cleaning debris was not captured and analyzed. Consequently, when the part was received at GE it was sent to the Strother engine services facility to perform a final clean and debris analysis. This cleaning was completed successfully with no non-conformances found.

The final task performed as part of the final single lot deliverable manufacturing process was the final dimensional inspection. The process entailed all dimensions specified on the 17A206-230 drawing being inspected for compliance. The results of the final inspections found a total of eight locations that did not meet the drawing specifications. Each of these locations was reviewed and found to not impact the part form, fit, or function and were accepted.

Images of the part after completion of all requirements specified on the drawing (17A206-230) can be seen in Figure 55 through Figure 57.


***Figure 55. 17A206-230G01 Final Single Lot Deliverable Part***


*Figure 56. 17A206-230G01 Final Single Lot Deliverable Part*

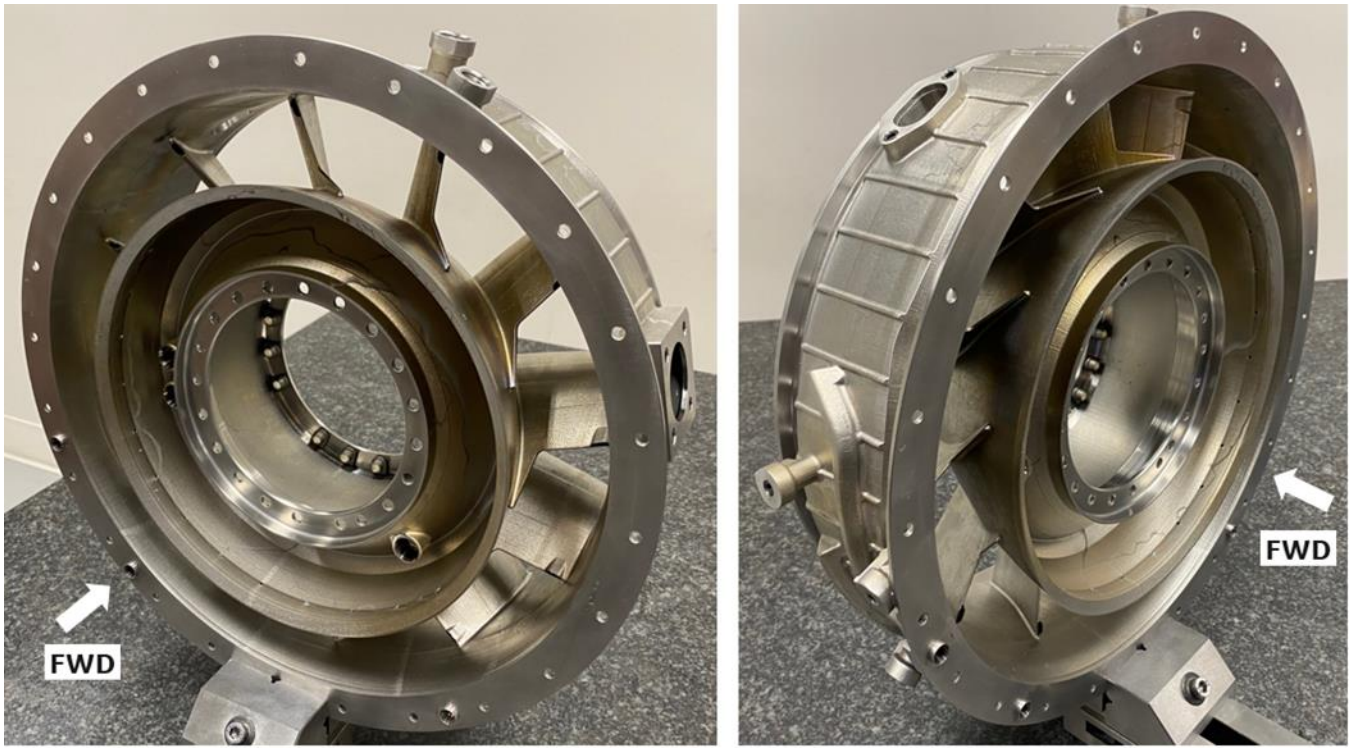


*Figure 57. 17A206-230G01 Final Single Lot Deliverable Part*

#### 3.2.5.3 Form & Fit Check-Out

The last requirement for the final single lot part was an assembly fit check. To accomplish this the final part was shipped to the U.S. Navy Patuxent River facility and installed onto a typical production T700-401C by Navy personnel using production DEPOT MAINTENANCE WORK REQUIREMENTS (DMWR) assembly instructions. Figure 58 through Figure 61 document the assembly of the Swirl Frame onto the engine. The final assembly was performed at the Navy PSEF facility and was successfully completed without issue. The Navy expressed interest in running the engine through a standard performance calibration after the installation of the final DDM Swirl Frame component. This performance calibration, if it occurs, would establish a TRL of 6 for the DDM Swirl Frame. The engine testing is outside the scope of this program and will be documented separately if it occurs.

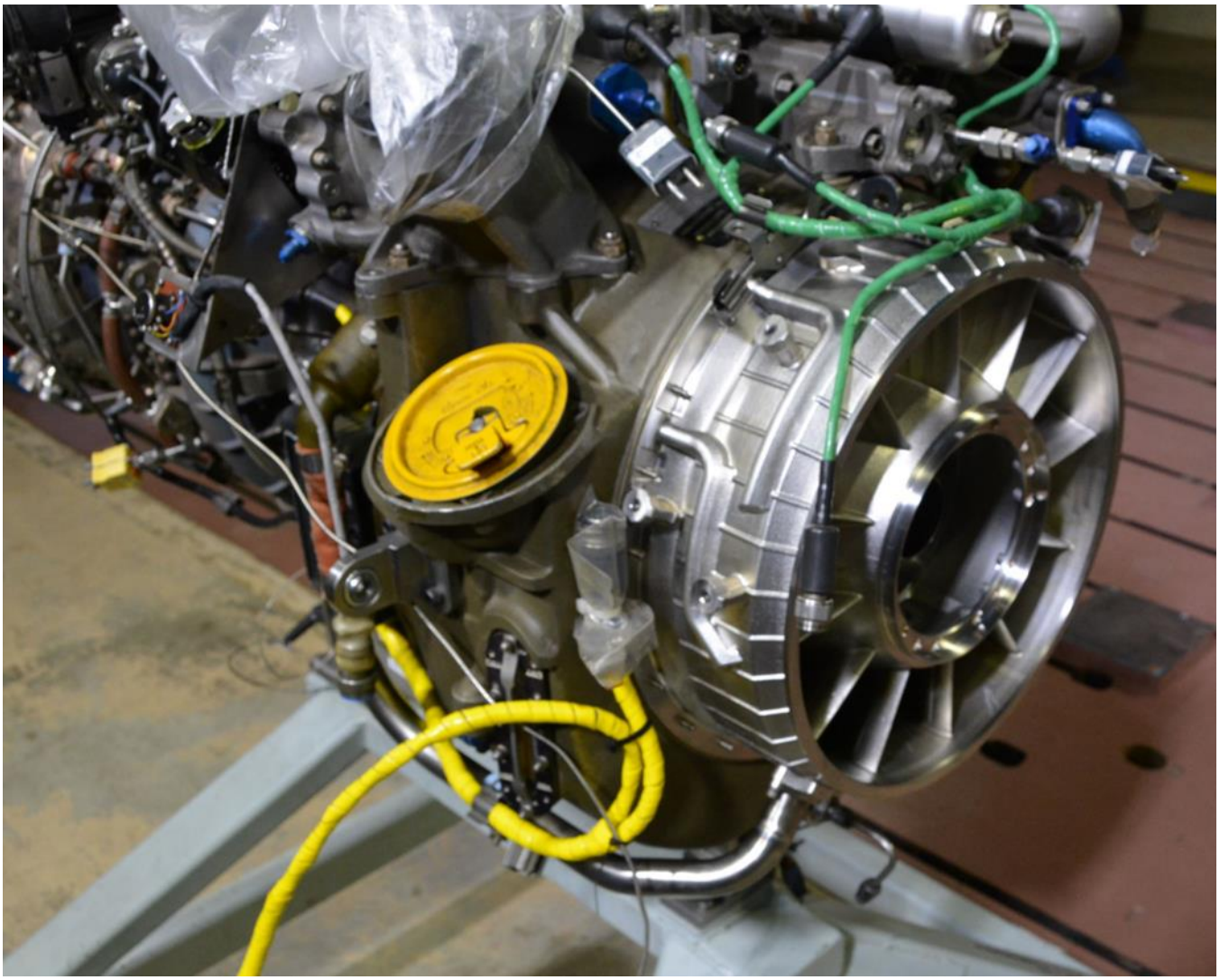

***Figure 58. Final Assembly Fit Check – 17A206-230G01 Additive Swirl Frame Installed on U.S. Navy T700-401C Engine***
*Photo courtesy of Naval Air Systems Command (NAVAIR)*

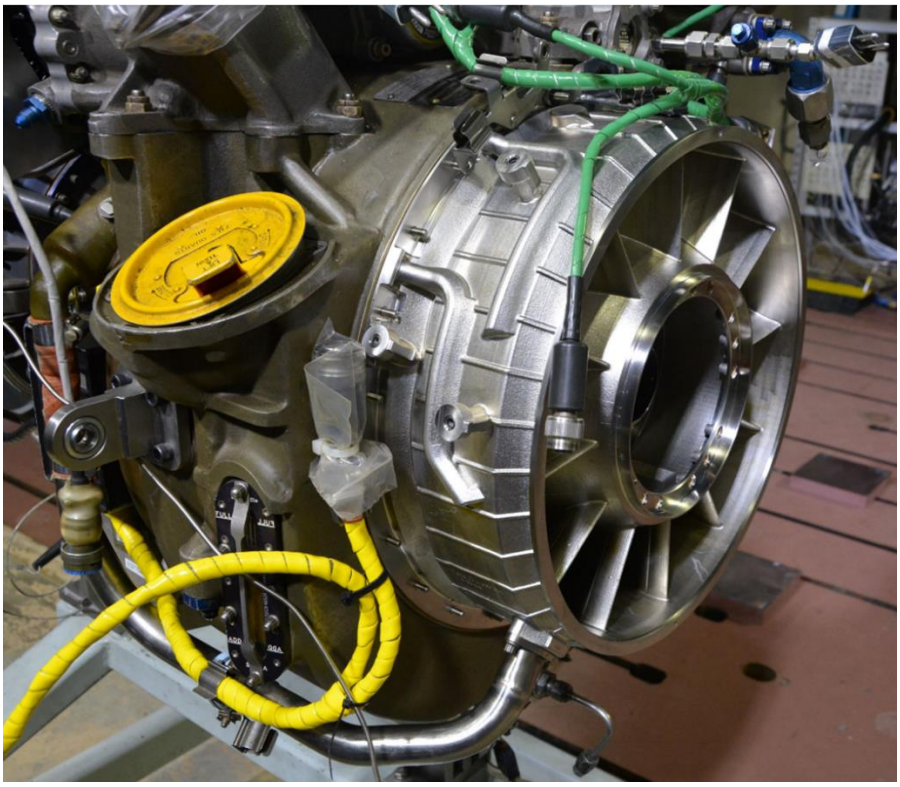

***Figure 59. Final Assembly Fit Check – 17A206-230G01 Additive Swirl Frame Installed on U.S. Navy T700-401C Engine***
*Photo courtesy of Naval Air Systems Command (NAVAIR*

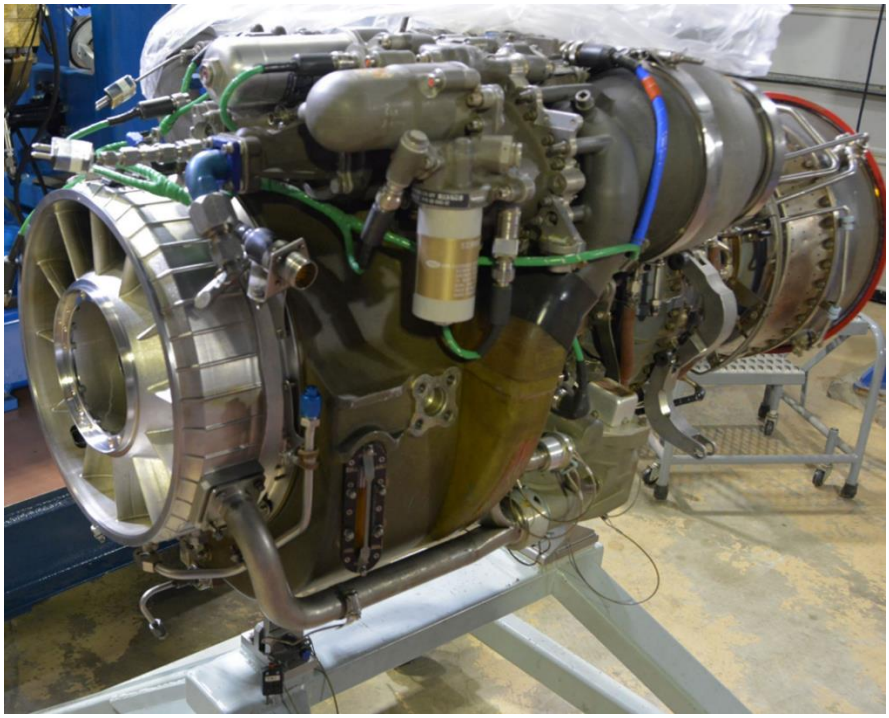

***Figure 60. Final Assembly Fit Check – 17A206-230G01 Additive Swirl Frame Installed on U.S. Navy T700-401C Engine***
*Photo courtesy of Naval Air Systems Command (NAVAIR*

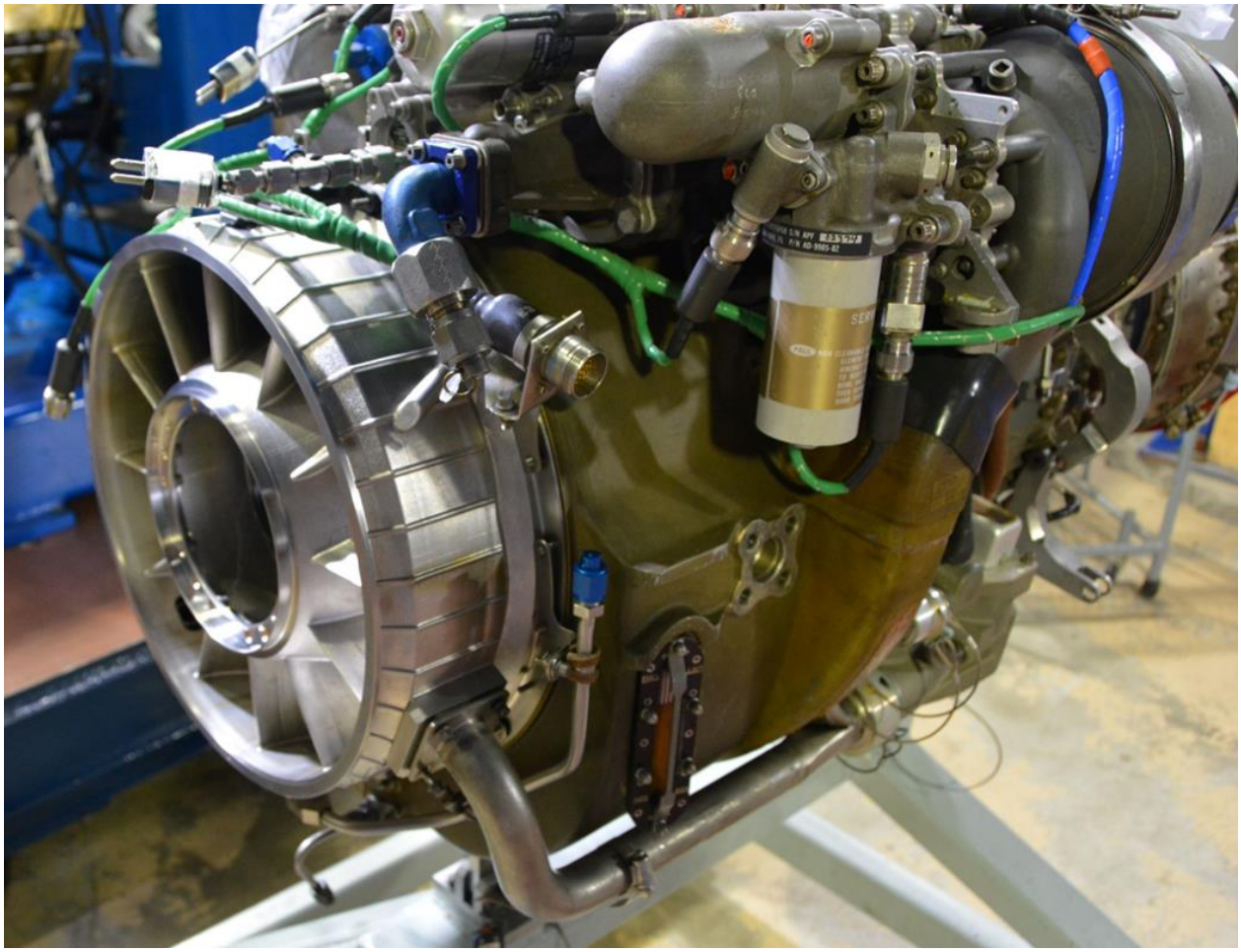

***Figure 61. Final Assembly Fit Check – 17A206-230G01 Additive Swirl Frame Installed on U.S. Navy T700-401C Engine***
*Photo courtesy of Naval Air Systems Command (NAVAIR)*

# 4. Conclusions

As discussed, this report covers the final phase of a four phase, $2.4M Army ManTech program to advance DDM processes for turbine engines. The program spanned candidate part selection, effects of surface finish on throughput, component build process development, DDM process development, DDM plan development, industrialization (part printing development) and finally engineering validation (final single lot part manufacturing).

All were successfully completed, with the results detailed in the earlier sections of the report. The capability to manufacture affordable aerospace quality DDM components was demonstrated and verified by the fabrication of sectors, full-scale trial builds culminating with a final engineering class full-scale single lot Swirl Frame manufactured on the ATLAS machine in IN718 for the T700 series of turboshaft engines used in the AH-64 and UH-60 helicopters.

The final full-scale Swirl Frame part was installed onto a typical production T700-401C by Navy personal at their Patuxent River facility successfully demonstrating form & fit of the final deliverable asset.

Along with the final single lot DDM Swirl Frame that was delivered at the end of this program, important learnings were realized in the areas of complex part printing, support structure strategies and post-processing activities. Details of these learnings can be found in Section 3.2.3. In addition to the part manufacturing learnings, significant findings were also documented in the areas of surface finish impact on throughput, multi-laser stitch evaluation, and melt pool sensing. Details of these learnings can be found in Section 3.2.2.

The successful completion of this project will help enable and optimize advanced AM processes for aerospace quality super-alloy engine components that will contribute to reduced costs, reduced weight and improved performance for the DOD, Department of Energy, and commercial sectors.

# 5. Project Benefits

With the goal of mission readiness as well as investigating cost savings measures, the DOD is the perfect organization to delve into the possibilities of DDM. With numerous aircraft in the fleet, both helicopter, fixed wing, and unmanned, there are a very large number of parts that would be candidates for DDM. In the maintenance and sustainment environment DDM could allow for streamlined inventory measures, quick part builds, and a much longer lifecycle for legacy as well as specialty equipment.

When the DOD can use the DDM process it not only saves time and money but also uses less invasive materials that need to be mined from the earth. In addition, raw materials aren't wasted because legacy equipment can be used for longer periods of time and funds allocated to new equipment could be used in mission critical operations. Successful completion and transition of the advanced DDM project described in this document will also enable a range of benefits to the warfighter including weapons systems availability, durability, customizability, efficiency, logistical support, costs, lethality, ease of maintenance, and safety.

Additionally, the use of DDM will save U.S. industries, especially the aircraft manufacturers and commercial airline companies' time, money, and productivity.

With the evolution of the DDM technology, the supply chain of parts will be disrupted forever, in a positive way. According to the Harvard Business Review, "Industrial 3D printing is at a tipping point, about to go mainstream in a big way. Most executives and many engineers don't realize it, but this technology has moved well beyond prototyping, rapid tooling, trinkets, and toys. 'AM' is creating durable and safe products for sale to real customers in moderate to large quantities."

With this change in business practices, and with the lower cost of doing business, a company may be able to lower their fees and become the preferred vendor making them more competitive in the global marketplace. Another way that companies can save resources with DDM is by elongating the lifespan of their equipment. Rather than purchasing whole new engines or other expensive parts because replacement parts are hard to acquire, with DDM specific parts could be manufactured Just-in-Time.

When companies have the ability to manufacture the needed part on their schedule and for less time and less cost there could be a whole mind shift in thinking about their processes. Personnel could have their skills upgraded and learn the DDM procedure and feel empowered within what was a routine position, thereby raising their quality of life.

Overall, the DDM advanced manufacturing technology is expected to have many positive impacts to both the DOD and the general public as it becomes more widely adopted within the aircraft industry.